

# **FUSION-BASED TECHNIQUES FOR IMAGE DEHAZING**

A DISSERTATION

SUBMITTED IN PARTIAL FULFILLMENT OF  
THE REQUIREMENTS

FOR THE AWARD OF THE DEGREE

OF  
**MASTER OF TECHNOLOGY**  
IN  
**SIGNAL PROCESSING AND DIGITAL DESIGN**

Submitted by:

**PAULAMI PURKAYASTHA**

**(2K21/SPD/09)**

Under the supervision of

**Dr. M. S. CHOUDHARY & Dr. MANJEET KUMAR**



**DEPARTMENT OF ELECTRONICS AND COMMUNICATION  
ENGINEERING**

**DELHI TECHNOLOGICAL UNIVERSITY**

(Formerly Delhi College of Engineering)

Bawana Road, Delhi-1100042

**MAY, 2023**

**DEPARTMENT OF ELECTRONICS AND COMMUNICATION  
ENGINEERING**

DELHI TECHNOLOGICAL UNIVERSITY

(Formerly Delhi College of Engineering)

Bawana Road, Delhi-110042

**CANDIDATE'S DECLARATION**

I, Paulami Purkayastha, Roll No. 2K21/SPD/09 student of M.Tech. (Signal Processing and Digital Design), hereby declare that the project Dissertation titled "Image Dehazing" which is submitted by me to the Department of Electronics and Communication, Delhi Technological University, Delhi in partial fulfilment of the requirement for the award of the degree of Master of Technology, is original and not copied from any source without proper citation. This work has not previously formed the basis for the award of any Degree, Diploma Associateship, Fellowship or other similar title or recognition.

Place: Delhi

PAULAMI PURKAYASTHA

Date:

**DEPARTMENT OF ELECTRONICS AND COMMUNICATION**  
**ENGINEERING**

**DELHI TECHNOLOGICAL UNIVERSITY**

(Formerly Delhi College of Engineering)

Bawana Road, Delhi-110042

**CERTIFICATE**

I hereby certify that the Project Dissertation titled “Image Dehazing”, which is submitted by Paulami Purkayastha, Roll No. 2K21/SPD/09 Department of Electronics and Communication, Delhi Technological University, Delhi in partial fulfillment of the requirement of the award of the degree of Master of Technology, is a record of the project work carried out by the student under my supervision. To the best of my knowledge this work has not been submitted in part or full for any Degree or Diploma to this University or elsewhere.

Place: Delhi

Dr M. S. CHOUDHARY

Dr MANJEET KUMAR

Date:

**SUPERVISOR**

**SUPERVISOR**

Professor

Assistant Professor

Electronics & Communication  
Bawana Road, Delhi-110042

Electronics & Communication  
Bawana Road, Delhi-110042

## **ACKNOWLEDGEMENT**

I would like to express my profound gratitude to Dr O. P. Verma Head of the Department of Electronics and Communication Engineering, for allowing the presentation of my Dissertation titled “Image Dehazing”.

I would like to express my special thanks to my guides Dr. M. S. Choudhary and Dr Manjeet Kumar for the time and effort that they provided throughout the project. Your useful advice and suggestions were really helpful to me during the project’s completion. In this aspect, I am eternally grateful to you.

I would like to acknowledge that this project was completed entirely by me and not by someone else.

Place: Delhi

PAULAMI PURKAYASTHA

Date:

## **ABSTRACT**

Image dehazing is a common term used to refer to the restoration, enhancement and de-blurring of images captured outdoors. It is a widely studied topic in literature and spans a large range of areas namely, outdoor surveillance cameras, satellite imaging, remote sensing, underwater imaging, object tracking, computer vision, etc.

Haze or corruption is a general term for the lack of clarity in an image when captured in moving/ low-light/ foggy conditions. Clarity here refers to good contrast, good lighting and good reflectivity of the object or scene, to be captured in the image. Atmospheric haze usually occurs due to multiple factors, especially in outdoor shoots, like dust, smoke, hailstorm, clouds and fog. Fog is an aerosol of water vapour and tiny ice crystals suspended in the air. In contrast to the general aerosol-type nature of the contamination, the case of haze in underwater images is an interesting topic to consider. Several authors consider the underwater haze similar to dense fog on land, but light below water is spectrally deprived. This happens because water redirects different wavelengths of light by different angles of refraction causing Spectral Distortion.

The Dissertation encompasses a review of the different means and techniques of image dehazing followed by a novel strategy to dehaze indoor and outdoor environmental images. The review on Image Dehazing Techniques first introduces haze in images, its types, causes and effects observed. The relevant literature is compiled and evaluated first. Following are the sections talking about the classifications of dehazing techniques in detail. Each sub-section lists the comparison of different papers for that particular class. A separate section just for the databases in common parlance helps the reader to select amongst available choices. Eventually,

the review includes the most recent research areas and topics under focus and finally draws out a relevant conclusion and charts a suitable goal area for research works.

Image dehazing by Image Enhancement focuses on improving the view of hidden objects in the image. On the other hand, Image Restoration in its fullest sense is a method that aims at re-doing or inverting the degradations performed on the image, that made it blurry in the first place. In a general sense, the Image Restoration method for Image Dehazing is a Restoration-Degradation model using a clear version of the image. Image Enhancement offers a significant advantage in the sense that it does not mandate the use of a template but, it is not efficient in case there is a vast array of images of the same area from different angles. Image Fusion then takes the lead because the method works by inculcating features from all available images of the scene/object under surveillance. Furthermore, in instances where images of a ‘moving’ object, like a human lung, growing cancer tumour, etc., are recorded, image fusion becomes necessary to combine all geometric transformations of the object to form a single master image.

The Dissertation introduces a novel method that uses Multi-Scale Image Fusion. The same is followed by another idea which combines the Retinex technique with Multi-Scale Image Dehazing so as to improve the results. The choice of the Retinex method is based on the fact that the output of the Retinex method mimics human vision and gives a good representation of the features of the hazy image. The star of the show is the simultaneous use of both the hazy and ground truth’s reflectance maps while performing fusion. The visual and quantitative comparisons of the present and previous works have also been performed and presented in this Dissertation.

# CONTENTS

|   |      |
|---|------|
| CANDIDATE’S DECLARATION .....   | I    |
| CERTIFICATE.....  | II   |
| ACKNOWLEDGEMENT.....  | III  |
| ABSTRACT .....  | IV   |
| CONTENTS .....  | VI   |
| LIST OF TABLES .....  | VIII |
| LIST OF FIGURES .....   | X    |
| CHAPTER 1 INTRODUCTION.....   | 1    |
| 1. FUSION-BASED TECHNIQUES FOR IMAGE DEHAZING.....  | 1    |
| LITERATURE REVIEW .....   | 1    |
| 2. STEERABLE PYRAMID BASED MULTI-SCALE FUSION ALGORITHM FOR<br>SINGLE IMAGE DEHAZING..... | 21   |
| 2.1 INTRODUCTION .....  | 21   |
| 2.2 RELATED WORKS .....   | 23   |
| 2.3 BACKGROUND THEORY.....  | 24   |
| 2.4 FUSION-BASED DEHAZING.....  | 25   |
| 2.4.1 <i>Derived Inputs</i> .....   | 25   |
| 2.4.1.1 White Balanced Image.....   | 25   |
| 2.4.1.2 Contrast-Enhanced Image.....  | 26   |
| 2.4.2 <i>Weight Maps</i> .....  | 27   |
| (i) Weight Map from Gaussian and Steerable Pyramid .....                                  | 27   |
| (ii)Weight maps from derived inputs:.....   | 28   |
| 2.4.3 <i>Multi-Scale Fusion</i> .....   | 29   |
| CHAPTER 3.....  | 30   |
| PROPOSAL-2 .....  | 30   |
| 3. A RETINEX PRIOR TO MULTI-SCALE FUSION FOR SINGLE IMAGE DEHAZING<br>30                  |      |
| 3.1 INTRODUCTION .....  | 30   |
| 3.2 BACKGROUND THEORY.....  | 32   |
| 3.3 MULTI-SCALE RETINEX BASED FUSION METHODOLOGY .....                                    | 32   |
| 3.3.1 <i>Multi-Scale Retinex</i> .....  | 32   |
| 3.3.2 <i>Normalized Weight Maps</i> .....   | 33   |
| 3.3.3 <i>Multi-Scale Fusion</i> .....   | 33   |
| 3.3.4 <i>Color Restoration</i> .....  | 34   |
| CHAPTER 4.....  | 35   |
| RESULTS AND DISCUSSION.....   | 35   |
| 4. IMAGE DEHAZING AND FUSION PYRAMIDS .....   | 35   |
| 4.1 STATEMENT ANALYSIS .....  | 35   |
| 4.1.1 <i>Why Fusion-based Image Dehazing?</i> .....                                       | 35   |
| 4.1.2 <i>Pyramidal Structure</i> .....  | 36   |
| 4.1.3 <i>Weight Maps</i> .....  | 36   |
| 4.1.4 <i>Multi-Scale Fusion</i> .....   | 36   |

|                         |   |            |
|-------------------------|---|------------|
| 4.2                     | QUALITATIVE RESULTS.....  | 36         |
| □                       | <i>Marked improvement in colour contrast</i> .....  | 39         |
| □                       | <i>Absence of Halo effects</i> .....  | 39         |
| □                       | <i>Clearer edge boundaries</i> .....  | 39         |
| □                       | <i>No Compression/pixel distortion</i> .....  | 39         |
| 4.3                     | QUANTITATIVE RESULTS .....  | 39         |
| <b>CHAPTER 5.....</b>   |   | <b>42</b>  |
| <b>CONCLUSION .....</b> |   | <b>42</b>  |
| <b>5.</b>               | <b>FUSION BASED TECHNIQUES FOR SINGLE IMAGE DEHAZING .....</b>                              | <b>42</b>  |
| 5.1                     | MOTIVATION .....  | 42         |
| 5.2                     | STATEMENT ANALYSIS .....  | 42         |
|                         | <i>Steerable Pyramid-based Multi-Scale Fusion algorithm for Single Image Dehazing</i> ..... | 42         |
|                         | <i>A Retinex prior to Multi-Scale Fusion for Single Image Dehazing</i> .....                | 42         |
| 5.3                     | OUTLINE .....   | 42         |
| 5.4                     | SIGNIFICANCE .....  | 42         |
| 5.5                     | CONCLUSION.....   | 43         |
| <b>6.</b>               | <b>REFERENCES.....</b>  | <b>425</b> |



# LIST OF TABLES

|                  |    |
|------------------|----|
| TABLE I .....    | 5  |
| TABLE II .....   | 7  |
| TABLE III .....  | 9  |
| TABLE IV .....   | 10 |
| TABLE V .....    | 11 |
| TABLE VI .....   | 13 |
| TABLE VII .....  | 16 |
| TABLE VIII ..... | 18 |
| TABLE IX .....   | 25 |
| TABLE X .....    | 26 |
| TABLE XI .....   | 37 |
| TABLE XII .....  | 39 |
| TABLE XIII ..... | 39 |

## LIST OF ABBREVIATIONS

| Abbreviation | Explanation   |
|--------------|---|
| AMBE         | Absolute Mean Brightness Error  |
| Ampl.        | Amplitude   |
| BRISQUE      | Blind/Referenceless Image Spatial Quality Evaluator                     |
| cGAN         | Cycle Generative Adversarial Network                                    |
| CLAHE        | Contrast Limited Adaptive Histogram Equalization                        |
| CNN          | Convolutional Neural Networks   |
| CT           | Curvelet Transform  |
| CVG-URG      | Computer Vision Group-University of Granada                             |
| CVPR         | Conference on Computer Vision and Pattern Recognition                   |
| DCP          | Dark Channel Prior  |
| FADE         | Fog Aware Density Evaluator   |
| FIR          | Finite Impulse Response   |
| FRIDA        | Foggy Road Image Database   |
| GIS          | Geographic Interphase System  |
| GT           | Ground Truth  |
| HF           | High Frequency  |
| I-HAZE       | Indoor Haze   |
| ITS          | Indoor Training Set   |
| LF           | Low Frequency   |
| MATLAB       | Matrix Laboratory   |
| MSCNN        | Multi-Scale Convolutional Neural Network                                |
| MSE          | Mean Square Error   |
| NIQE         | Naturalness Image Quality Evaluator                                     |
| NTIRE        | New Trends in Image Restoration and Enhancement                         |
| OTS          | Outdoor Training Set  |
| PSNR         | Peak Signal to Noise Ratio  |
| RESIDE       | Realistic Single Image Dehazing   |
| SSIM         | Structural Similarity Index   |
| USC-SIPI     | University of Southern California-Signal and Image Processing Institute |
| WT           | Wavelet Transform   |

## LIST OF FIGURES

|   |    |
|---|----|
| FIGURE 1 – CLASSIFICATION OF HAZE IN IMAGES .....     | 2  |
| FIGURE 2-DEHAZING ALGORITHMS IN COMMON PARLANCE ..... | 3  |
| FIGURE 3-‘DEGRADATION-RESTORATION’ MODEL.....         | 8  |
| FIGURE 4-ATMOSPHERIC SCATTERING MODEL.....            | 24 |
| FIGURE 5-WEIGHT MAPS.....                             | 28 |
| FIGURE 6-WEIGHT MAPS FROM DERIVED INPUTS .....        | 29 |
| FIGURE 7-RETINEX WEIGHT MAPS.....                     | 33 |
| FIGURE 8-FUSION PYRAMID .....                         | 34 |

# CHAPTER 1

## INTRODUCTION

### 1. FUSION BASED TECHNIQUES FOR IMAGE DEHAZING

#### LITERATURE REVIEW

##### Introduction

Image dehazing is a common term used to refer to the restoration, enhancement and de-blurring of images captured outdoors. It is a widely studied topic in literature [1], [2], [3], [4] and spans a large range of areas namely, outdoor surveillance cameras, satellite imaging, remote sensing, underwater imaging, object tracking, computer vision, etc.

Haze or corruption is a general term for the lack of clarity in an image when captured in moving/ low-light/ foggy conditions [5]. Clarity here refers to good contrast, good lighting and good reflectivity of the object or scene, to be captured in the image. Figure 1 compiles a flow chart of different types of hazes that have been observed in the domain of image de-hazing. Atmospheric haze usually occurs due to multiple factors, especially in outdoor shoots, like dust, smoke, hailstorm, clouds and fog. Fog is an aerosol of water vapour and tiny ice crystals suspended in the air. Atmospheric haze can be classified as either reflection haze or transmission haze [6] as shown in Figure 1. When too much light is reflected from the photographed object, the object seems to be a white blur of light and contrast adjustments become a necessity to better the clarity. This type of haze is called reflection haze. Haze removal in this case targets reducing contrast and sharpening the background. Similarly, in transparent and translucent objects like lenses, light scattering is negligible, so detecting the boundaries becomes a tough task. Haze in such a case is the contamination observed due to refraction from the first surface and reflection from the second one. Likewise, object-tracking or computer vision applications include visual surveillance and digital forensics. Factors like rain, smog, hailstorms, forest burns, low lighting, etc. cause blurring of captured images in this case.

In the case of Earth's observation satellite imagery or remote sensing applications, the haze is the blurring caused due to atmospheric suspended particles and aerosols that cohere together to form thick clouds that loom in the air [7] [8]. These suspended clouds are the result of long-term air polluting practices like incorrect disposal of chemical gases, the gaseous residue of burnt fuels, forest fires, volcanic eruptions, mine blasts and suspended dust particles that cling together to form molecular 'smog' in dry air. Other factors include meteorological phenomena like mist [9]. However, the mist is a combination of ice particles and condensed vapour, the dust particles act

as coagulants and create a condensation-nuclei hence, creating a wet haze [5]. Satellite Imagery for planet or meteor exploration also suffers from haze issues caused due to photo-chemical interactions (see Figure 1) in the upper atmosphere of planets and comets that result in halos around objects [10]. Dehazing such images are tougher comparatively because of their high contrast natures. Another aspect of regularity studied by a team of professors studying Saturn’s Hexagon, observed by NASA’s CASSINI Spacecraft, is in the distribution of the hazes in the planet’s atmosphere when seen vertically [11]. It suggests that the gravity waves are responsible for the vertical hazes. Such hazes produce oscillations in density and also affect the temperature of the atmosphere. This is a well-known phenomenon on Earth and on other planets, which results in blurring.

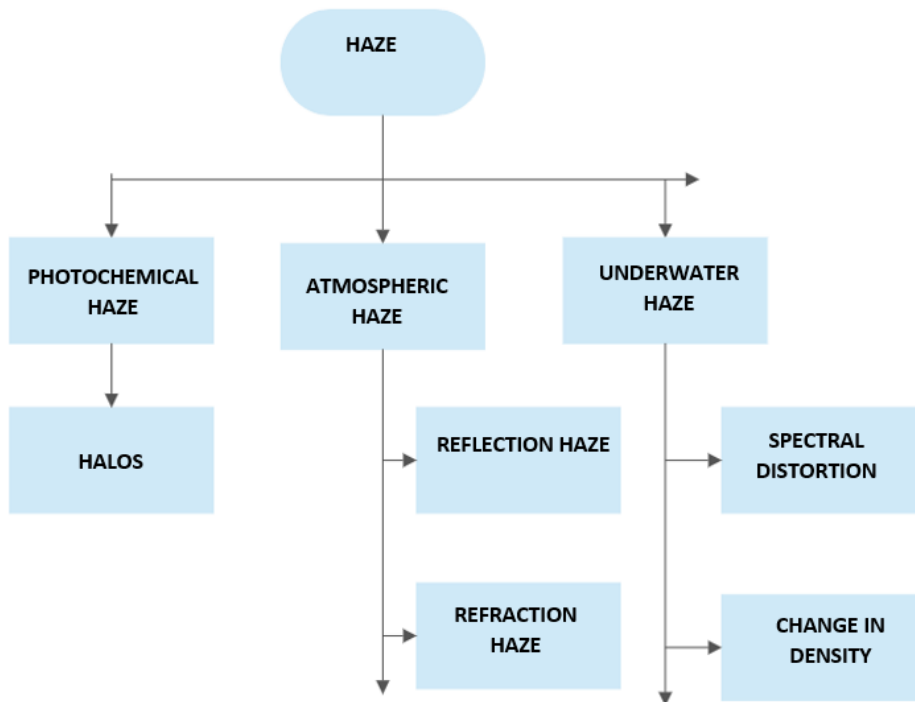


Figure 1 – Classification of Haze in images.

In contrast to the general aerosol-type nature of the contamination, the case of haze in underwater images is an interesting topic to consider [12]. Several authors consider the underwater haze similar to dense fog on land, but light below water is spectrally deprived. This happens because water redirects different wavelengths of light by different angles of refraction causing Spectral Distortion (refer to Figure 1). The degree of incidence and the ratio of refraction indices determine the degree of refraction for a particular wavelength of light, as stated by Snell’s law [13], [14] [15]. In nature, we have different levels of salinity in sources of water. The Euhaline seas have salinity in the range of 30-35 %. Similarly, the brackish seas and metahaline seas are saline (0.5 - 29 % & 36-40%) [16], [17], [18]. The point to note here is that water tends to vary in salinity seasonally making spectral distortion a seasonal phenomenon. Salinity in bodies of water generally ranges from freshwater to brine creating a wide niche for such studies in the literature. Due to the salt and particle content, light becomes scarce due to multiple scattering, similar to the Tyndall effect

[19] making it the major cause of spectral distortion underwater. As can be observed from Figure 1, another cause of underwater haze lies in variations in density as we delve deeper into the water body due to temperature. Just as the temperature reduces with depth, the density of water increases causing light to get more and more refracted. This happens because of the inverse proportionality of the refractive index and temperature [20], [21], making the travel of photons tougher underwater. Other factors include the addition of pollutants into the sea causing eutrophication or algal bloom [22] which reduces visibility by the release of toxins and colored pigments in fresh water. This paper aims to study image dehazing techniques in common use and frame a review of relevant papers in this domain. This paper includes a study of major image de-hazing techniques and creates a comparison to formulate a guide to choosing dehazing algorithms based on the depth of haze in the image.

### Dehazing Algorithms in Common Parlance:

The number of different dehazing algorithms has been increasing at a steady pace in the past few years. With the increasing availability of datasets and the ease of implementing techniques on them via Python, MATLAB etc.

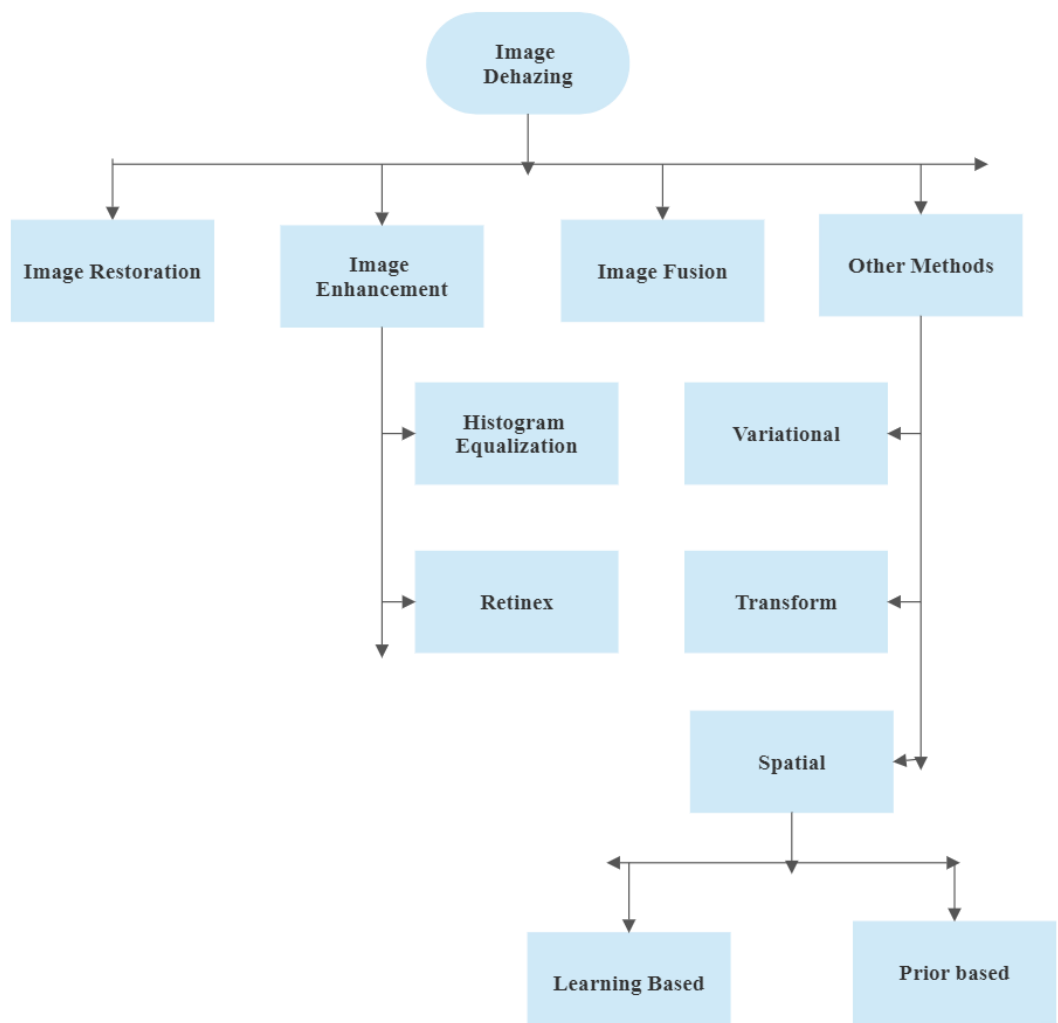


Figure 2-Dehazing Algorithms in common parlance

Image-processing software and languages, there is a necessity to list down all methods at one place. This review paper is an attempt to create a ready reference for any image-dehazing enthusiast and lists down methods in common parlance in an orderly fashion. The flow chart in Figure 2 is an overview of the techniques collected in this paper.

#### *Dehazing by Image Enhancement*

Atmospheric image enhancement generally includes preprocessing images such that original data content increases. The method comes under the category of prior-based spatial domain dehazing. One of the key features is the independence from depth-map. Hence, even when the physical estimations are violated, the algorithm does not suffer. Some common ways are filtering with morphological operators, histogram equalization, noise removal using filters, linear contrast enhancements, etc.

#### Histogram Equalization

A digital image has a histogram with the level of intensity  $[0, L-1]$ , as given in equation (1), which is a function with discrete values;

$$H(t_k) = n_k \quad (1)$$

Where  $n_k$  represents a number of pixels with intensity  $t_k$ . The horizontal axis intensity is given by the values of  $t_k$  representing the  $k^{\text{th}}$  intensity level, while the vertical axis is given by the value of  $n$ ;

$$n = MN \quad (2)$$

Where, the dimensions of the image are  $M \times N$ .

$$p(t_k) = \frac{n_k}{n} = \frac{n_k}{MN} \quad (3)$$

Thus, histograms are  $h(r_k)$  vs  $n_k$  plots or  $p(r_k)$  vs  $r_k$  plots [23].

Numerous spatial-domain evaluating techniques form the basis for histograms. Manipulating histogram are used to achieve better image contrast and hence the enhancement of the image [24]. Local histogram-equalization methods are better than global-methods because of greater image detailing in local patches and thus a stronger performance [25], [26]. The paper by Yeh [27], proposes a histogram separation algorithm. According to the paper, a combination of multiple thresholding and PSNR is done to beneficially segregate histogram-bins and preserve mean-brightness. Xu & Zhai for their paper [28], propose an equalization model to achieve the best contrast result by trading off contrast with color tone. Another paper by Wang and Zhu, [29], uses histogram equalization followed by nonlinear enhancement of coefficients. The coefficients are obtained from wavelet transform. The Contrast Limited Adaptive Histogram Equalization (CLAHE) method is prevalent in literature including [30] and [31]. The paper [30] combines the CLAHE technique with that of the filter technique of Weiner filter and the paper [31] combines the same with the FIR decomposition filter.

### Retinex Method

Another popular method is the Retinex method that has the principle that intensity ‘L’ is the multiplication of illumination ‘Il’ with reflectance ratio ‘RR’, stated in equation (4) cited from [24]:

$$L(x, y) = Il(x, y) \times RR(x, y) \quad (4)$$

Here, if  $f(x,y)$  denotes 2-dimensional picture, then, the image intensity ‘L’ or gray level, is the amplitude of function ‘f’, ‘Il’ denotes illumination of the object at coordinates  $(x,y)$  and ‘RR’ denotes the ratio of reflectance. To tackle the variation in illumination, we can remove illumination ‘Il’ from the equation (4) by taking logarithm of the complete equation (4),

$$\log(L(x, y)) = \log(Il(x, y)) + \log(RR(x, y)) \quad (5)$$

On subtracting the first term from equation (5), we get the pure reflectance parameter  $RR(x,y)$ .

Consequently,  $RR(x,y)$  is called Retinex output,

$$\log(RR(x, y)) = \log(L(x, y)) - \log(Il(x, y)) \quad (6)$$

Literature on retinex method focus on preprocessing the Original Image and replacing the gaussian smoothening stage with other methods [32], [33]. The retinex approach on its own is not sufficient in dehazing accurately and so is often combined with other techniques. One example for the same is the paper by Tang, Yang, He [34] wherein they have found two transmission maps, one draft estimated by Retinex and other found by Dark Channel Prior (DCP) method. To obtain a final haze-free estimation, the two are combined by fusion. The paper by Tian and Li [35] uses U-net and highlights the usability of deep-learning methods in image processing for transmission depth independent spatial methods of image dehazing.

**TABLE I**  
**COMPARATIVE STUDY OF PAPERS STUDIED UNDER IMAGE ENHANCEMENT-BASED DEHAZING METHODS**

| <i>Ref.</i> | <i>Method</i>                 | <i>Year</i> | <i>Database</i>             | <i>Metrics</i>                                    |
|-------------|-------------------------------|-------------|-----------------------------|---|
| [25]        | Histogram Segmentation        | 2014        | CVG-URG database            | Kruskal-Wallis test                               |
| [26]        | Enhancement of 2-D Histogram. | 2011        | USC-SIPI, Kodak Image Suite | Kruskal-Wallis test and computational complexity. |
| [27]        | Multiple thresholding         | 2013        | Set of Random Images        | Absolute Mean Brightness Error                    |



|      |   |      |  |   |
|------|---|------|--|---|
|      | procedure on histogram.                               |      |  | (AMBE), PSNR, Time Complexity                         |
| [28] | Joint Contrast Enhancement                            | 2014 | Berkeley Segmentation Dataset (BSDS300)                | The increase in visible edges, Mean visibility level. |
| [29] | Histogram Equalization followed by Wavelet Transform. | 2013 | Large data set of Natural Hazy Images.                 | Ampl(%), Loss(%), Time Complexity                     |
| [30] | CLAHE & Weiner Filter                                 | 2015 | Real images of outdoor scenes                          | Block size, Stepsize, Gamma correction factor.        |
| [32] | Particle Swarm Optimization & Retinex                 | 2020 | Natural Images   | PSNR, SSIM  |
| [33] | Fuzzy-based Retinex                                   | 2017 | Mobile Computer-Database, AR face database             | EER(Face Recognition Error), ANSP                     |
| [34] | Incorporating Taylor Series with Retinex in DCP       | 2020 | MSCNN-HE   | PSNR, SSIM, CIEDE2000                                 |
| [35] | Deep Dehazing Retinex network                         | 2020 | RESIDE-ITS, RESIDE-OTS, (I-HAZE, O-HAZE and DENSE-HAZE | SSIM, PSNR  |

#### *Dehazing by Image-Fusion*

Image-fusion is an approach focused on combining multiple images to form a single image. The fundamental research area for the same is to determine the best algorithm to combine the images. The common practice is to either combine multispectral images (multispectral imaging captures data of image within specific wavelengths across the spectrum) or a single-images for fusion to enhance the original image. First, two images are to be aligned so that the pixels are in corresponding positions. Next, the images are decomposed using frequency or wavelet transforms of choice. The H-H, H-L, L-H and L-L sub-bands are thus obtained at the coarsest level. Except for the low-low band, all other bands have non-positive values corresponding to the “salient features” of the image indicating the edges, troughs and lines. As a result, it is always better to integrate the greater absolute value out of the two for each pixel location and

thus perform fusion. Lastly, we perform an inverse transform to get a dehazed image. The paper [36] uses two modified versions of the original image and weighs them by specific maps, then carries out fusion-based image modification. Another paper by the same author, takes the concept one step further by using Multi-Scale Fusion technique. As given in [37], they compute three weighting maps containing weights of luminance, chromaticity, and saliency and then reduce irregularities and multiscale, by using a Laplacian pyramid. In the paper [38], the encoder captures input images, while the decoder captures outputs. The outputs are computed after passing the test image through the trained network. The constructed network has a fusion plan of finding inputs from the test hazy image. This is done by first White Balance, secondly Contrast Enhancing, finally, Gamma Correction. Lastly, pixel-based confidence maps are computed to preserve good color visibility. The papers, list out the importance of fusion in image dehazing applications. For underwater enhancements too, image fusion works well as shown in [39]. For color images, the FWT using weights technique suggested by [40] is efficient.

**TABLE II**  
**COMPARATIVE STUDY OF PAPERS STUDIED UNDER IMAGE FUSION-BASED DEHAZING METHODS**

| <i>Ref.</i> | <i>Method</i>                                | <i>Year</i> | <i>Database</i>                  | <i>Metrics</i>  |
|-------------|--|-------------|----------------------------------|---|
| [36]        | Fusion based                                 | 2010        | Natural hazy Images              | Amplitude (%), Loss(%)                                    |
| [37]        | Multi-Scale Fusion                           | 2013        | Natural Hazy Images              | Visual Inspection and method used by Hautere et all. [41] |
| [38]        | Deep-Learning network using fusion           | 2018        | -                                | -   |
| [39]        | Contrast enhancement followed by Fusion      | 2013        | Random Images                    | MSR   |
| [40]        | Fast Wavelet Transform Weighted Image Fusion | 2014        | Tiananmen, Train, Cannon7, House | Time, Edge, Gradient.                                     |

#### *Dehazing by Image restoration*

Under this aegis, restoring a noisy image is the main idea. Noise can be blurred due to motion, mis-focus in camera, noise [42]. It is conducted by identifying and inverting the system function that corrupted the picture. It is done by using the “Point Spread Function” to recover the picture data lost to corruption. Image restoration is not equal to image enhancement because the latter is enacted to increase the number

of features of the picture. While, image-restoration tries recovering lost data, but of course, image enhancement followed by restoration improves image quality highly. The degradation and restoration model can be easily visualized using Figure 3.

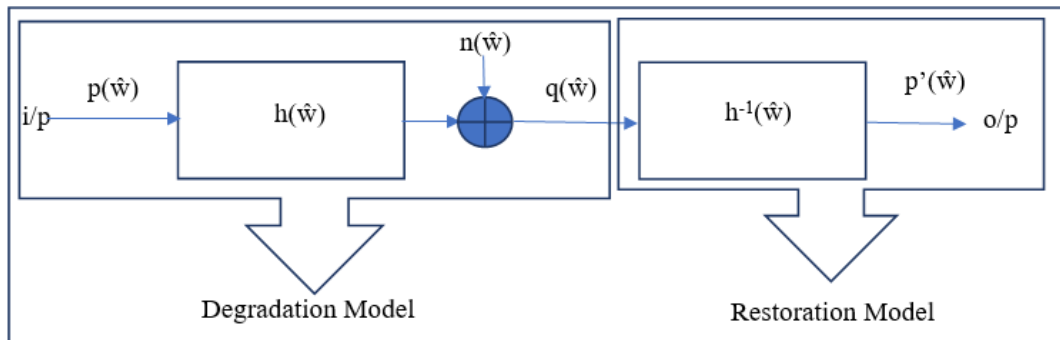


Figure 3-Image Restoration algorithm explained using 'Degradation-Restoration' model [44]

However, the drawback of the model is quite significant. The given strategy ignores external conditions such as fog, mist or smoke denoted by  $n(\hat{w})$  and simply takes the inverse of system function  $h(\hat{w})$ . Though in simple terms, image-restoration means restoring a degraded image but practically such a solution is not actually effective. To remove haze completely, we need machine learning technique incorporated into it. The method used by [44] explores 'haze-relevant' features like presence of multiple scaled darkened channel  $D$ , multiple scaled local maximum contrasted feature  $C$ , hue-disparity  $H$ , multiple scaled local maxima saturation  $S$ . They train a random-forest classifier with these features extracted from a clear reference to de-haze a synthetically generated hazy-image. Compared with the standard method proposed by Kaiming He, et. al [45] of DCP this method, when compared to [44], shows that the latter eliminates the risk of over-dehazing and has a lesser Mean-Square Error (MSE) due to the added effect of regression. Another method by Gibson et. al [46] interpolates the image in high-resolution using a Markov network model and provided an image in low-resolution so to form the super-resolution image. Zhu et. al gives a prior that is a color-attenuated version of the above method given in two back-to-back papers [47], [48]. In that technique, a linear single model for scene depth is formed as below:

$$d(x) = \theta_0 + \theta_1 v(x) + \theta_2 s(x) + \varepsilon(x) \quad (7)$$

Where, 'd' is haze depth and  $x$  is the location within image,  $v$  is brightness and  $s$  is saturation, ' $\theta_0$ ', ' $\theta_1$ ', ' $\theta_2$ ', are linear coefficients and ' $\varepsilon(x)$ ' is an arbitrary error.

Images with 120 sample points each were chosen. A set of 500 training images were used to train a Supervised Learning Model for creating an abyss mapping for hazy image. Using the feedback of the model, the depth information is achieved and consequently removed from the image. However, this relies heavily on training data. The similar approach can be iterated to use for multiple images and thus subsequently remove haze from frames of videos too. Another method approaches the problem by setting thresholds for contrast of an image. The two conditions used are that the de-hazed image should have contrast greater than the hazy image and secondly, that the edges or boundaries of the enhanced image should merge smoothly with the background [49]. The method removes haze by increasing the local divergence of a single picture & can result in a "Halo effect" due to sudden changes in depths. Based

on similar techniques, [50] later proposed a dehazing method that considers local contrast and spatial distribution to generate local features.

TABLE III

**COMPARATIVE STUDY OF PAPERS STUDIED UNDER IMAGE RESTORATION-BASED DEHAZING METHODS**

| <i>Ref.</i> | <i>Method</i>   | <i>Year</i> | <i>Database</i>                      | <i>Metrics</i>                                |
|-------------|---|-------------|--------------------------------------|---|
| [44]        | Extracts some haze-relevant features from training data to estimate transmission map.   | 2014        | Synthetic Images                     | MSE   |
| [45]        | Restores image using DCP Method   | 2009        | An outdoor image set from flickr.com | Visual Inspection                             |
| [46]        | Estimating depth from fog in a single image by interpolating patches of images taken from different directions.   | 2013        | FRIDA                                | Visual Inspection                             |
| [47]        | Calculates gradient of image to create depth-map.   | 2014        | Google Images and Flickr             | MSE, SSIM, Time Complexity, Visual Inspection |
| [48]        | Continuation of [47]  | 2015        | Google Images and Flickr             | Image Size                                    |
| [49]        | Removing the lightness in color of the input by estimating chromaticity to improve contrast. Finally using pixel information to build Markov Random Fields to get Airlight. | 2008        | Real Images of outdoor scenes.       | Visual Inspection                             |
| [50]        | Scale Invariant Feature Transform points (SIFT) are searched in difference of gaussian scale space.   | 2014        | Real Hazy Images                     | Overlap Error                                 |

## Other Dehazing Algorithms

### *Variational Domain*

The methods in this domain extract the transmission map on basis the variation in inter and intra channel pixels. The paper by Hasil Park [51], expresses the transmission map as a function of product of mean of pixels extracted from different channels in the image. The explanation for the constituent terms shows how the transmission map is driven by the changes in the gradient of the picture, in other words, variations. The foggy regions get transcribed into the map and are indicative of the energy transformation in the work by Shu et al. [52] the foreground is used to generate the first transmission map. It is then imposed on the second one created from the sky regions using weighted-fusion method. To optimize it, a proposal of a variational model is given, which, in combination with Koschmeider's method, provides a dehazed output. Another work by Kang and Jung [53] uses an alternating (colour and grey) transmission map and incorporates it into an inter-channel framework used for generating a correlation term. The term thus generated is used in the proposed variational model.

**TABLE IV**  
**COMPARATIVE STUDY OF PAPERS STUDIED USING**  
**VARIATIONAL DOMAIN**

| <i>Ref.</i> | <i>Method</i>   | <i>Year</i> | <i>Database</i>           | <i>Metrics</i>      |
|-------------|---|-------------|---------------------------|---------------------|
| [51]        | Fuzzy membership function, L1-norm-based regularization.  | 2017        | 4 Random Hazy Images      | CNR, NIQMC, Entropy |
| [52]        | Weighted fusion based coarse transmission map estimation followed by regularization.                | 2019        | Degraded Realistic Images | PSNR, SSIM          |
| [53]        | A 'Alternate minimization algorithm' is applied to a combination of Atmospheric and Retinex models. | 2020        | RESIDE 2016               | PSNR, SSIM          |

### *Transform Domain*

In Transform Domain we have two kinds of techniques. Curvelet Transform and Wavelet Transform. Wavelet Transform (WT) works similar to homomorphic filter. The image is first distributed to different frequency sub-bands, Low-Frequency (LF) and High-Frequency (HF). Then the frequency sub-blocks that are not in lower frequency range, are enhanced. Curvelet transform (CT) improves WT by also covering multi-scale aspects of the image. Verma *et al.* [54], combined the CT and Multiple Polynomial Regression Model (MPRM). The intermediate step of obtaining depth-map of the image is performed using MPRM in their paper. [55] Khan *et al.* used WT in their paper and used HF bands to estimate airlight. The LF bands are used to dehaze the image using reconstruction. [56] Fu *et al.* perform 2D discrete WT

(DWT) on the image and subsequently pass it through a generative Adversarial Network (GAN). The overall technique is named namely DW-GAN. The DWT branch of the dual-branched network, utilizes WT and gets feature maps. The second branch prevents over-fitting issues using ImageNet. ImageNet is a pre-trained Res2Net network. The drawback of WT is that it is not useful in over-bright, over-dark, or unevenly illuminated images. [57] Hsu and Chen address this problem by developing a multi-scale network. Their method segments the image into 3 HF and 1 LF component followed by wavelet denoising. The fusion of cleaned sub-images gives dehazed output. [58] Hodges *et al.* in their cascaded dehazing-discriminating network improve training performance. Since the dehazing network is driven by the error (network loss curve), the algorithm gives a better performance than its counterparts. However, LF sub-bands are rarely worked upon in these papers. [59] Liu *et al.* in their paper, suggest an open dark channel model (ODCM). The claim is that ODCM minimizes the haze of LF areas. Soft-thresholding is employed to reduce the noise. The haze-free image is wavelet-recreated by fusing improved LF. Another method that addresses LF sub-band is the method by [60] He *et al.* In their paper, LF sub-band is optimized using a linear function to un-complicate the process. However, the method highly reduces performance.

**TABLE V**  
**COMPARATIVE STUDY OF PAPERS STUDIED IN TRANSFORM DOMAIN**

| <i>Ref.</i> | <i>Method</i>                             | <i>Year</i> | <i>Database</i>  | <i>Metrics</i>   |
|-------------|---|-------------|--|--|
| [54]        | WT and dense haze elimination.            | 2019        | Online Synthetic dataset of natural images   | MSE, PSNR, SSIM, RMSE and MAE                                    |
| [55]        | 2-D WT and GAN                            | 2021        | RESIDE-ITS, NTIRE19, NTIRE20, NITRE21  | PSNR, SSIM   |
| [56]        | 2-D DWT with Wavelet Denoising by filters | 2021        | O-Haze, I-Haze   | PSNR, SSIM   |
| [57]        | Deep Learning based network               | 2019        | Training:<br>Google searches, KITTI dataset, Youtube Images<br>Testing:<br>RESIDE/SOTS, RESIDE/RITS, NITRE18 | SSIM, PSNR, COCO Map, Time complexity                            |
| [58]        | WT followed by DCP and Soft Thresholding  | 2017        | Natural Hazy image   | Visible edge, Gradient & Saturated pixel ratios, Time complexity |
| [59]        | 2-D Multi scale WT                        | 2017        | Natural Hazy Images  | Visible edge, Gradient & Saturated pixel                         |

|      |                            |      |   |                         |
|------|----------------------------|------|---|-------------------------|
|      |                            |      |   | ratios, Time complexity |
| [60] | Multilevel WT optimization | 2019 | “Canyon”, “Desk”, “Hill”, “House”, “Lily”, “Mountain”, and “River” images | MSE, SSIM, PSNR         |

### *Spatial Domain*

The methods under spatial domain image processing involve applying direct operations on the pixels of the image. The process starts with dividing the image space into uniform pixels according to their spatial coordinates. Each pixel is a unit having specific intensity and resolution. Majorly, the areas of research that have been most popular to dehaze images, largely fall under spatial domain and hence the methods used in common parlance listed before are also its part. Since, the use of deep-learning based methods have proved excellent for dehazing purposes, they have often been combined with the techniques to give desired results. Consequently, the sub-techniques under this domain can be classified as learning-based or without learning-based (Prior based).

### Learning Based

Learning-based techniques can be categorized on the basis of the data training approach adopted by the researcher. Further, the network type and parameters that are estimated shape the overall methodology.

### Supervised Learning

Supervised learning networks work by finding intricate details in the input dataset by creating computational models having multiple processing layers of abstraction. Convolutional Neural Network (CNN) is a type that uses pixels to learn and thus classify images’ features. In an image, Airlight( $A$ ), Radiance( $R$ ), and Transmission maps ( $T_x$ . map) are indicative to the presence of haze. Cai *et al.* [61] developed an end-to-end dehazing network. The novel network called DehazeNet predicts  $T_x$  map. Along with it,  $A$  is considered to be the 0.1% of the darkest pixels of  $T_x$  map. Koschmeider equation gives an easy dehazed solution on basis estimated  $A$  and  $T_x$  map. Here, the authors also develop a new activation function called Bilateral Rectified Linear Unit (BReLU). A more developed approach to CNN is the Residual-CNN. Employing the same, Li *et al.* [62] propose a simple 2-phase network. The first phase estimates  $T_x$  map while the second induces dehazed image basis the residue. Advancing further on the idea of increasing CNN layers, Yuan *et al.* [63] suggest DehazeNet. The network is multi-scale in nature and contains multiple hierarchical levels of learning. The proposal in their paper essentially combines Network-in-Network (NIN) with Multi-Scale CNN (MSCNN), forming NIN-DehazeNet. Another example of multi-scale CNN is the paper by Ren *et al.* [64]. The method of this paper applies dual networks, one fine and another coarse to estimate  $T_x$  maps, one detail and the second local respectively.

Inspite of the increasing accuracy of  $T_x$  maps estimated, final dependence stays with the Koschmeider’s equation. A model superior to Koschmeider’s is proposed by Deng *et al.* [65] which estimates both  $A$  and  $T_x$  map. called Haze-Aware Representation

Distillation GAN (Hard-GAN). The absence of suitable  $A$  training datasets is the sole drawback. Xiao *et al.* [66], in their paper, suggest the addition of a separate dehazing layer that removes block artefacts and halos from the image. This eliminates the need to estimate  $A$ . High time complexity and failure to dehaze heavy-haze are the limitations suffered by this method. The CycleGAN formulation of Engin *et al.* [67] provides a method other than Residual-CNN to incorporate residue in the dehazing network. If we try and eliminate the dependence on Koschmeider’s equation, prior-based methods can be utilized. Su *et al.* [68] attempt to dehaze an image with the use of a prior-based dehazing network called conditional GAN (cGAN). The core idea behind cGAN is to learn a mapping function between hazy and clear images directly guided by latent encoding information in the prior-based dehazed image.

#### Semi-Supervised Learning

The supervised category trains on synthetic content that imitates haze while the unsupervised category learns from real hazy images. In semi-supervised learning, both branches of the network share weight as in the paper by Li *et al.* [69]. Their method uses both synthetic and real-world data to improve versatility. The use of multi-level multi-scale block is also predominant in the field when we consider semi-supervised learning. Wang *et al.* [70] introduce a weakly supervised framework that predicts the Tx map,  $A$ , as well as an intermediary dehazed result. Optical flow ground truths of hazy images are employed in the paper by Yan *et al.* [71]. Iteration is used to train both supervised and unsupervised dehazing networks using the same set of images. Fusion of the results of the 2 sub-branches gives dehazed image. An *et al.* [72] extend this by employing encoding–decoding neural network for the branch with supervised learning. Two similar sub-networks (A-net, T-net) are implemented in the unsupervised branch that finds the Tx map and  $A$ . The only drawback of this sub-domain is the dependency on haze-free ground truths for training.

#### Unsupervised Learning

The major limitation of supervised and semi-supervised versions of learning-based dehazing is the mandatory requirement of such a dataset that has its corresponding label. So, just for comparison, a few methods of the unsupervised category have been presented here. The framework by Hodges *et al.* [58] is an example. A fine example of post-processing is another paper by Qu *et al.* [73], which develops Enhanced Pix2pix Dehazing Network (EPDN) using GAN. The output of the GAN is passed through an enhancer which improves color and other features. The performance metrics calculated in the paper include PSNR, SSIM and Perceptual Index (PI).

TABLE VI

COMPARATIVE STUDY OF PAPERS STUDIED USING LEARNING BASED IMAGE DEHAZING METHODS

| <i>Ref.</i> | <i>Method</i>             | <i>Year</i> | <i>Database</i>                       | <i>Metrics</i>          |
|-------------|---------------------------|-------------|---------------------------------------|-------------------------|
| [61]        | DehazeNet and BReLU       | 2015        | Random haze free images from internet | MSE, SSIM, PSNR, WPSNR  |
| [62]        | CNN and Residual learning | 2018        | NYU2 Depth dataset                    | PSNR, SSIM, FSIM, SSEQ, |



|      |  |      |   |  |
|------|--|------|---|--|
|      |  |      |   | BRISQUE,<br>NIQE                               |
| [63] | NIN-DehazeNet,<br>MSCNN                            | 2019 | NYU2 Depth,<br>Middlebury stereo,<br>RESIDE | PSNR, SSIM                                     |
| [64] | Multi-Scale Deep<br>Neural Network                 | 2019 | NYU2 Depth dataset                          | PSNR, SSIM,<br>MSE                             |
| [65] | Hard-GAN   | 2020 | NTIRE 2020                                  | PSNR, SSIM,<br>LPIPS                           |
| [66] | Novel Haze removal<br>layer & CNN                  | 2020 | Middlebury stereo                           | PSNR vs<br>Iteration graph                     |
| [67] | CycleGAN   | 2018 | NTIRE18, NYU<br>Depth                       | PSNR, SSIM                                     |
| [68] | cGAN & Prior-based<br>CNN                          | 2021 | RESIDE ITS &<br>SOTS, HAZERD,<br>NTIRE18    | PSNR, SSIM,<br>CIEDE2000,<br>Visual Inspection |
| [69] | Semi-Supervised<br>CNN                             | 2020 | RESIDE-C,<br>HazeRD, SOTS, ITS,<br>OTS      | PSNR, SSIM,<br>RTTS, mAP%,<br>run-time         |
| [70] | Multi-Scale, Multi-<br>Level Deep CNN              | 2020 | TrainA, RESIDE-<br>SOTS, RTTS &<br>HSTS     | PSNR, SSIM,<br>CIEDE2000                       |
| [71] | Domain<br>transformation and<br>Optical flow model | 2020 | vKITTI and author-<br>collected dataset     | EPE, Bad Pixel                                 |
| [72] | Supervised branch,<br>A-net, T-net                 | 2021 | RESIDE & HSTS                               | FADE, PSNR,<br>SSIM                            |
| [73] | EPDN   | 2019 | RESIDE-SOTS                                 | PSNR, SSIM, PI                                 |

#### Prior Based

Without learning-based methods depend on assumption or prior knowledge. The use of prior estimates extracted from the input image are ingredients of the image dehazing hierarchy, hence we call it the Prior-based method.

#### Depth-Map Estimation

Depth estimation measures distance of pixels from a central point in a monocular (single) or set of stereo (multiple views of a scene) image. Geometrical disparities were often the subject to calculate depth traditionally, however, newer techniques minimizing the regression loss for the same. Learning frames or object placing sequentially is also a technique employed for estimating depth. The map created basis displaced pixels is called depth-map. The Dark Channel Prior (DCP) was first coined by He et al. [74]. The critical observation that states that the sky regions have pixel values with very low intensity in at least one-color channel is the main principle behind this method. Mathematically, DCP expressed as [74]:

$$J^{dark}(x) = \min_{m \in \Omega} \left( \min_{c \in \{R,G,B\}} (J^c(m)) \right) \quad (8)$$

Here  $\Omega$  is the local path centered at  $m$ ,  $J$  is an input image  $J^{dark}$  is the dark channel of  $J$ . Based on DCP, a rough transmission map is estimated using [74]:

$$t(x) = 1 - \min_{m \in \Omega} \left( \min_{c \in \{R, G, B\}} \left( \frac{I^c(m)}{A^c} \right) \right) \quad (9)$$

Where  $I$  is the degraded image,  $t(x)$  represents the transmission map and  $A$  is the airlight. The assumption that DCP is not suitable for sky images implies that refinement of the transmission map is needed, which requires high computations. The reason for such an assumption is the presences of blocky artifacts in the dehazed result. The work by Colores et al, [75] performs normalization prior to applying DCP to target removal of artifacts. A better method proposed by Dai et al. [76], on Robust Atmospheric Scattering model (RASM), modifies the DCP by adding a noise term in the original equation to tackle blocky effect caused due to reflectance. The method also adds a compensation term that tackles deep-haze region

Meta-heuristics

In the area of global optimization, a large number of Metaheuristic Algorithms (MA) had been proposed over the years for complex engineering issues. It is common to observe that MAs emulate processes and behaviors inspired by mechanisms present in nature, such as evolution. Those used in this area range from clustering to edge and region growing. The paper by Vinay Chopra et al. [77], suggests Brightness Channel Prior (BCP) based dehazing model, where, a Nondominated Sorting Genetic Algorithm improvises gradient filter. Another paper by V. J. D. Almero et al. [78] suggests dehazing by DCP extended to underwater images. The parameter values, allotted in this paper are based on a Genetic Algorithm (GA) of chromosome encoding.

*Filtering Based*

Typical methods used in this sub-domain include homomorphic filtering, Wavelet Transform (WT) and Curvelet Transform (CT). The paper by Tan et al. [79], agrees that Single-Scale Retinex (SSR) algorithm is good for color illumination but suffers Halo effect in case of uneven lighting conditions in the image. Resolving the issue, firstly, the smog in the image is processed by SSR. A modified Gaussian homomorphic filter is then employed for Halo. CLAHE algorithm is the final step in this paper that ensures good visibility by removing noise. For underwater images, the paper by Yu and Lou [80], propose combining three steps of homomorphic filtering, double transmission map and dual-image wavelet fusion. Considering filter-based dehazing, work on underwater images is more in number nowadays. The paper by Yu, Li, Lou and Yan [81], focuses on color accuracy analysis and uses homomorphic filtering as a pre-processing step to their non-convex optimization. WT & CT are just 2 sides of a coin and both are used as an advanced step to homomorphic filtering. A technique combining deep learning and WT is suggested in the paper [82]. The other version replacing WT with CT can be seen in [83].

TABLE VII

## COMPARATIVE STUDY OF PAPERS STUDIED USING PRIOR -BASED IMAGE DEHAZING METHODS

| <i>Ref.</i> | <i>Method</i>   | <i>Year</i> | <i>Database</i>   | <i>Metrics</i>  |
|-------------|---|-------------|---|---|
| [74]        | DCP   | 2011        | Images from popular search engines and Flickr                       | Distributions of average and cumulative pixel intensity   |
| [75]        | Scattering model applied to DCP                           | 2019        | 22 Random Images  | PSNR, SSIM  |
| [76]        | RASM  | 2019        | RESIDE, O-HAZE, FADA  | PSNR, SSIM, SSEQ, BLINDS-II, CIEDE2000  |
| [77]        | BCP   | 2021        | Author collected  | Percentage of saturated pixels, haze gradient, contrast gain, visible edges, execution time, SSIM, PSNR |
| [78]        | DCP & Theory of Natural Selection (GA)                    | 2020        | 3 images from aquaculture setup                                     | MSE, PSNR, SSIM   |
| [79]        | SSR & CLAHE   | 2019        | DukeMTMC-reID database  | mAP   |
| [80]        | CLAHE, double transmission map, dual-image wavelet fusion | 2020        | 5 Underwater Random Images  | UCIQE, Entropy, average Gradient  |
| [81]        | CLAHE & Color Line model                                  | 2022        | Photos taken at the Zhangzi island subsea breeding base from China. | UCIQE, UIQM   |
| [82]        | Wavelet U-Net and Chromatic adaptation transform          | 2019        | RESIDE  | SSIM, PSNR  |
| [83]        | Curvelet Transform followed by Histogram Equalization     | 2019        | Single Random Image   | SSIM, PSNR  |

## Recent Research Areas

*Computational Photography*

Computational Photography is the domain of imaging that focusses on improving image-capturing devices by making them mechanically more versatile. The major

idea behind the field is the need to shift the dependency from original image dehazing algorithms. Another attractive prospect is the advantage of getting highly-defined images without the need for extensive post-processing. The field earmarks conventional morphological operations performed on images and gives incentives to create their mechanical equivalents. Research work in this domain include Microsoft Research: Real-Time Hyperlapse Creation Via Optimal Frame Selection [84], which presents an algorithm to click clear images even at high-frequency moving conditions of the camera. The technique in reality, tries to tackle hyperlapse-a condition of timelapse in presence of shaky hand-held capture. This paper is a successor of [85], another of Microsoft's research.

#### *Variational Autoencoders*

There are two major families in deep generative domain of deep learning, the first being GAN and the other is Variational Autoencoders(VAE). Autoencoders are basically cascaded encoders and decoders whose input and result should be same and is a proof for lossless encoding. The feature of VAE is that the weights of the networks are updates after each process by considering the errors between the input and result. The so called errors are nothing but variations and hence the name VAE. The same process is iterated until lossless encoding objective is achieved. The paper by Microsoft's Wan and Zhang [86], builds on the same principle and contains a dual VAE network. One branch caters to clean real-world old images and the other to their corrupted versions. The translation between the two branches is achieved using synthetic image pairs. The major advantage of the framework is that it allows the network to work even with real datasets with the same accuracy as observed during test, which guarantees "Generalization".

#### *Imagen*

The Imagen [87] is a model presented by Google Research: Brain Team. It performs text-to-image translations using a diffusion framework. With respect to text-image alignment, the algorithm achieves an FID score of 7.27 on COCO dataset without ever training on it. Imagen contains of an encoder network that maps to a diffusion model, which are gaussian processes. The same are sampled using classifier-free guidance, a method that samples randomly without depending on any classifier. But, this sampling is iterative and often results in unnatural images. Hence, dynamic thresholding is applied and the final result is obtained.

#### *Image Inpainting*

Image Inpainting is the technique to fill in the gaps of an image. The gaps are the spaces that either do not contain pixels, that is, are absent from the image, or spaces that have gotten destroyed due to age. The main principle behind the technique is to copy the pixels from the neighboring regions and pasting them in the gaps, such that the geometry and life-like aspect of the objects in the image remains unaltered. Such a technique is similar to the morphological operation of zooming, called interpolation in technical terms and results in a greater area coverage. The major difference

between the two is that interpolation does not guarantee merging between two pixel-vacant areas but Image Inpainting does. The paper by Adobe Research: [88], is an outstanding proof of the same, it proposes a GAN framework to design an object-aware training scheme that performs semantic-aware structure synthesis followed by spatial modulation, to fill in the gaps in the input image. Another paper working on similar principles is Adobe Research: [89], that superimposes the face of the person over a full-length picture of another person without any trace of discoloration or photoshop pixel-cracks. The crux of the paper is Image inpainting again but not for pixel-absent gaps but for dissimilar pixels in the original and superimposed faces. The GAN tries to match and thus change the facial/ hair features of the original person to that of the superimposed image, that way creating a new image.

#### Datasets

The table below lists out some datasets used in common parlance along with their features and references.

**TABLE VIII**  
**LIST OF COMMONLY USED DATABASE**

| <i>Ref.</i> | <i>Method</i>  | <i>Year</i>         | <i>Database</i>  |
|-------------|--|---------------------|--|
| [90]        | CVG-URG database   | 2014                | Biomedical, Astronomical, color and grey level PBM images.   |
| [91]        | University of Southern California- Signal and Image Processing Institute. (USC-SIPI) | -                   | Brodatz textures, Aerial images and some sequences(Moving head, fly-overs, moving vehicles).   |
| [92]        | Kodak Image Suite  | 1999 (Last Use)2013 | Lossless full color (24 bits per pixels) images in PNG format.   |
| [93]        | Berkeley Segmentation Dataset (BSDS300)  | 2007                | 30 humans were clicked to obtain 1000 coral images. Combining both color and grayscale version segmentations, 12,000 images are there in total.                                |
| [94]        | University of South Florida. Digital Mammography Database (USF-DM)                   | 2006                | More than 2600 digitalized mammography, classified and commented   |
| [95]        | AR-Face Database   | 1998 (Last use)2010 | 126 people whose 4000 color images have been clicked with different lighting and expression over 2 sessions.   |
| [96]        | RESIDE   | 2019                | ITS (Indoor Training Set), OTS (Outdoor Training Set), SOTS (Synthetic Objective Testing Set), RTTS (Real-world Task-Driven Testing Set), HSTS (Hybrid Subjective Testing Set, |

|       |   |                        |  |
|-------|---|------------------------|--|
|       |   |                        | Unannotated Real-world Hazy Images   |
| [97]  | RESIDE- $\beta$ and STANDARD  | 2019                   | Modified RESIDE-OTS, -RTTS, Unannotated Real-world Hazy Images.  |
| [98]  | Foggy road Image Database (FRIDA) & FRIDA2  | 2010 - 2012            | FRIDA and FRIDA2 contain synthetic image datasets having 90 and 330 images respectively, The images are of foggy road scenes taken from driver's perspective.  |
| [99]  | FLICKR  | -                      | Public dataset of Images at FLICKR   |
| [100] | New Trends in Image Restoration and Enhancement (NTIRE) [NTIRE16 [101], NTIRE17 [102], NTIRE18 [103], NTIRE19 [104], NTIRE20 [105], NTIRE21 [106], NTIRE22] | 2016-till present Year | It is a body conducting workshops and challenges for emerging trends in domain of image restoration and enhancement. Every year, it is held at different locations and new datasets are provided for the challenge purposes. |
| [107] | KITTI   | 2013                   | The KITTI Vision Benchmark suite is a project of Karlsruhe Institute of Technology and Toyota Technological Institute at Chicago. It uses autonomous driving platform, Anniway to get the images for 3-D vision.             |
| [108] | NYU2  | 2012                   | This comprises of frames of indoor scenes. The videos are recorded using Microsoft Kinect. They are captured in the RGB and Depth transmission maps.   |
| [109] | Middlebury Stereo   | 2001-2021              | Contains multiple groups of datasets recorded in the years 2001, 03, 05, 06 14 and 21. The topics of the images are not fixed but different.   |
| [110] | DukeMTMC-reID database  | 2016                   | Duke Multi-Tracking Multi-Camera ReIDentification is the largest available pedestrian dataset.   |
| [111] | FADE  | 2014-2015              | Fog aware Density Evaluator is a metric proposed by The University of Texas at Austin. It is a   |

|  |  |  |  |
|--|--|--|--|
|  |  |  | framework comprising test images<br>to defog foggy images. |
|--|--|--|--|

## CHAPTER 2

### PROPOSAL-1

#### 2. STEERABLE PYRAMID BASED MULTI-SCALE FUSION ALGORITHM FOR SINGLE IMAGE DEHAZING

Multi-Scale Fusion Technique employs different versions of the image to be dehazed to extract haze-relevant parameters that aid in image dehazing. The method proposes a variant of the technique using a Steerable Pyramid. The proposed method extracts steer-coefficient matrices from the original hazy image and incorporates them into the multi-scale fusion algorithm. The proposed technique aims to reduce the halo effect observed in image-dehazing applications and related works. Moreover, the work aims at the quality improvement of the output image by the novel algorithm it proposes. Quantitative, as well as a visual display of results, using the I-HAZE dataset, give an accurate interpretation of the effectiveness of the proposed work.

##### 2.1 Introduction

Images captured in real life are often found to be, blurred, smokey or low in contrast. The noisy characteristic of such an image is called ‘haze’ in image processing terminology and the method to remove haze from images is called Image Dehazing. Atmospheric dust, pollution, water vapor, smog, low lighting and shaky photography are some causes of haze. A ‘Clear Image’ has sharp object boundaries, good contrast and has been taken under good lighting conditions. Forensic photography, satellite imaging, remote sensing, record keeping, robotic vision, etc., are some of the areas that cannot function without a clear image. This fact along with the growing advancements in photo-editing, journaling and drones, make Image Dehazing a prime area of research.

The vast research on Image dehazing can be categorized based on the ‘dehazing process that is followed by the researcher. The flow chart of Figure 1 gives a brief idea about the different image dehazing approaches available in the literature. Under the aegis of image dehazing by Image Enhancement, the research area mainly focuses on improving the view of hidden objects in the image. The paper by B. Soni et al. [5], uses Contrast Limited Adaptive Histogram Equalization (CLAHE) method followed by an FIR Decomposition filter to dehaze hazy images. Another sub-branch of Image enhancement is the Retinex method employed in papers like [6] and [7], which make use of bio-inspired algorithms and fuzzy logic, respectively, in their modification of the Retinex method. The next category of Image Dehazing is dehazing by Restoration which is different from Image Enhancement, because, the latter does not require the researcher to know the exact degradations plaguing the image.



Image Restoration in its fullest sense is a method that aims at re-doing or inverting the degradations performed on the image, that made it blurry in the first place. In a general sense, the Image Restoration method for Image Dehazing is a Restoration-Degradation model [8]. The paper by Kaiming He et al. [9], was a landmark in this category, since, the mainstream method of Dark Channel Prior (DCP) was first introduced in their paper. The method first finds a depth map corresponding to the non-sky patches in the image and then extracts a dark channel (DCP) from it. The dark channel defines the pixels that have abnormally low intensities and which form the transmission map. The papers by Tang et al. [10], explore haze-relevant characteristics of the hazy image and discover a multi-scale dark channel, hue-disparities, etc. and remove them to obtain a clear image. Image Restoration, however, mandates the use of a transmission map/ depth map/ image prior for image dehazing. Image Enhancement offers a significant advantage in this sense but, it is not efficient in case there are multiple images of the same scene or object just like in the case of the databases of Geographic Interphase System (GIS), where, there is a vast array of images of the same area from different angles and depth. Image Fusion then takes the lead because the method works by inculcating features from all available images of the scene/object under surveillance. Furthermore, in instances where images of a ‘moving’ object, like a human lung, growing cancer tumour, etc., are recorded, image fusion becomes necessary to combine all geometric transformations of the object to form a single master image.

The inspiration of this method is taken from Ancuti et al. [1] and Dalvi et al [2] and aims to modify the procedure by using a Steerable kernel. From the previous works in literature, it is observed that most works extract weight maps from the original input and then derive coefficient matrices from them. These matrices thus generated, provide the required multi-image scenario for image fusion [11-14]. The methodology proposed inculcates information from the original input along with the coefficients derived from weight maps as inputs to the fusion pyramid structure. This work transmits the original image via a steerable pyramid [3] to obtain ‘Steer Coefficients’. The coefficients are passed through a Gaussian pyramid and correspondingly a matrix called a steer-gauss map is achieved. Additionally, Contrast-Enhancement and White balancing operations are performed on the input image to generate two corresponding weight maps. The weight maps and the steer-gauss map are used to generate a final weight map that acts as an input to the Laplacian pyramid. Finally, a fusion of the images as suggested by Ancuti et. al. [1] is performed to get the dehazed output. Therefore, this multi-scale fusion technique uses all three types of pyramid kernels and the coefficients from the unaltered image input, to compute the dehazed fusion image. The multi-scale fusion technique has been adopted because it helps in recovering hidden information from the original hazy image and is more efficient than the Image Enhancement and Restoration categories. Further, the steer coefficients derived from the hazy image prevent any loss of information that may arise while extracting contrast-enhanced and white-balanced coefficient matrices. The Gaussian pyramid is a smoothing pyramid that removes the characteristic ‘halo’ observed around objects in the steer coefficient matrix. The Laplacian kernel is used to enhance the edges around the objects present in the image. In the proposed method,

the Laplacian pyramid technique is used twice, once while computing corresponding weight maps of contrast-enhanced and white-balanced coefficient matrices and second, while generating the fused image. Further, normalization is performed before transmitting via the different kernels to avoid artefacts. The proposed technique is a per-pixel technique and thus does not need to estimate airlight (light reflected from nearby objects/secondary sources) for every region in the image. Moreover, since most techniques assume uniform airlight throughout the scene (which is not true in real-life), inaccurate results are a frequent occurrence. Hence, the proposed technique is said to maintain the originality of the scene through the airlight-free technique of fusion. This advantage stems from the fact that the proposed technique does not depend on Koschmeider's model for Image Dehazing. Also, the method proposed is efficient and independent because it derives all its weight maps from the single hazy image provided and does not need a transmission map for computations. The dataset I-Haze [4] is selected to test the algorithm proposed. The dehazed result has been compared with the previous methods in literature and performance metrics like PSNR, BRISQUE etc. are calculated and compared with previous related papers.

## 2.2 Related Works

The fundamental research area for Image Fusion focuses on determining the best algorithm to combine the images and the best scale-space representation of the images. The common practice is to either combine multispectral images or form a single image for fusion to enhance the original image. First, two images are to be aligned so that the pixels are in corresponding positions. Next, the images are decomposed using frequency or wavelet transforms of choice. The High-High (H-H), High-Low (H-L), Low-High (L-H) and Low-Low (L-L) sub-bands are thus obtained at the coarsest level. Except for the low-low band, all other bands have non-positive values corresponding to the "salient features" of the image indicating the edges, troughs and lines. As a result, it is always better to integrate the greater absolute value out of the two for each pixel location and thus perform the fusion. Lastly, an inverse transform gives a dehazed image. The paper [11] uses specific maps to weigh the image and then creates a fusion using the resultant weights. Another paper by the same author takes the concept one step further by using the Multi-Scale Fusion technique that employs using more than one version of the original image. As given in [1], they compute three weighting maps containing weights of luminance, chromaticity, and saliency and then reduce irregularities. In the paper [12], the encoder captures input images, while the decoder captures outputs. The outputs are computed after passing the test image through the trained network. The constructed network has a fusion plan of finding specific inputs from the test hazy image. This is done by first White Balance, second Contrast Enhancing, and finally, Gamma Correction. Lastly, pixel-based confidence maps are computed to preserve good colour visibility. These papers list the importance of fusion in image dehazing applications. For underwater enhancements too, image fusion works well as shown in the paper [13]. For colour images, the FWT using the technique of the weight as suggested by [14] is efficient. It is noteworthy that the research on fusion pyramids for Image Dehazing started with the landmark paper by Andelson & Anderson et al [15] which introduced the pyramid methods to process images. Since then, many

types and combinations of kernels have been explored for pyramids, of which, the most popular (used in [11] & [1]), is the gaussian kernel in which gaussian filters are used to smoothen the pixels as a step in pyramid generation stage. In this pyramid, blurring gives the next level, which is again blurred to form subsequent levels. This method ensures that each pixel corresponds to the local average of its neighbours in the lower level. The gaussian pyramid is nothing but a chain of down-sampling operations. The next type of kernel is the Laplacian kernel which is a slight modification of the gaussian kernel in the sense that here each level has a laplacian coefficient which equals the difference of levels in the gaussian pyramid. Though these definitions prove to be quite simple, however, the computations involved require an upscaling of the smaller image to allow subtraction between the two levels. The Laplacian pyramid is just a low-frequency vestigial of the gaussian pyramid. Both of the kernels defined above employ only one kernel at each subsequent step. The Steerable Pyramid method, suggested by Simoncelli et al. [3], is an advancement that employs a multi-scale pyramid having multiple directional orientations. In other words, it can be thought of as a band-pass filter bank which is an orientation-specific version of the Laplacian pyramid.

### 2.3 Background Theory

Luminance is the directional intensity of light rays emitted from an object. In case of the presence of an external light source, It is the light which gets reflected from the object or objects in the scene under consideration and enters the camera lens. The Image Degradation model or Atmospheric Scattering model relates the attenuation of luminance, through the atmosphere, with the degraded image. If  $I(x)$  is the degraded image and  $J(x)$  is its restored version, then, the Atmospheric scattering model gives the following equation;

$$I(x) = J(x)t(x) + A(1 - t(x)) \quad (10)$$

Where  $t(x)$  stands for ‘direct transmission’ and ‘A’ is the Airlight of the scene.

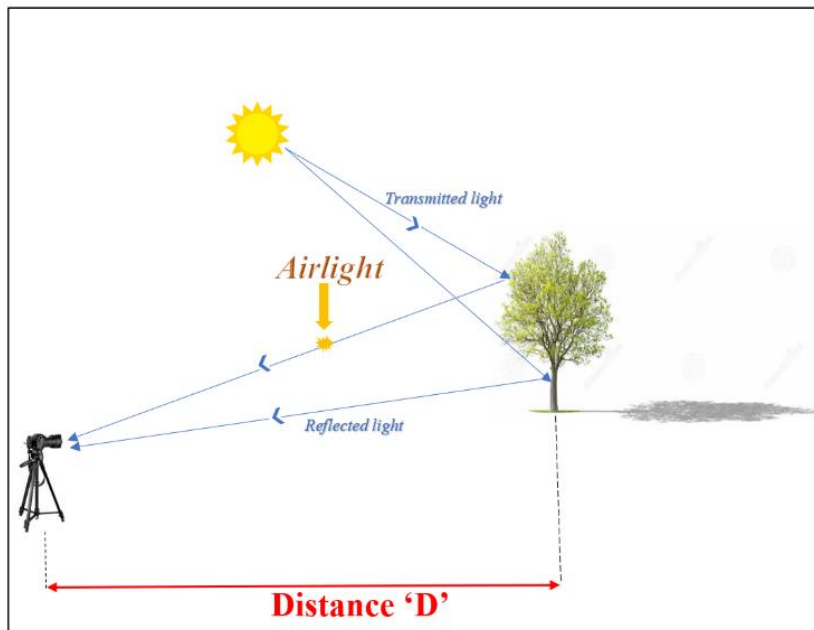


Figure 4-Atmospheric Scattering Model

The ‘direct transmission can be defined with the help of the atmospheric scattering coefficient ( $\beta$ ), which is a parameter governing the amount of scattering suffered by the rays reflected by the object.

$$t(x) = e^{\beta d} \quad (11)$$

Where  $d(x)$  is denoted by ‘D’ in Figure 4. The other parameters used can be visualized in the adjoined Figure 4.

## 2.4 Fusion-Based Dehazing

### 2.4.1 Derived Inputs

#### 2.4.1.1 White Balanced Image

In real life, on a camera-clicked picture, the unnatural shade of blue overlaying the real colors is pretty evident. This tone of color is not visible to the naked eye because the brain generally compensates for this unnaturalistic phenomenon. However, for the camera-taken pictures, the employed technique is called white balancing. Note that, during the white balancing process, we have to technically adjust the colors along two spectrums; the blue-yellow spectrum, also known as the color temperature and the green-magenta spectrum, also known as the color tint.

TABLE IX

ALGORITHM 1: ALGORITHM TO CONSTRUCT WHITE BALANCED IMAGE

---

|   |  |
|---|--|
| <b>Input:</b> RGB Components of Hazy Image; $\{Im = [R \ G \ B]\}$              |  |
| <b>Output:</b> White Balanced RGB Components; $\{Im_{wb} = [R_w \ G_w \ B_w]\}$ |  |
| 1.  | <b>Step 1:</b> Compute the average of RGB components (Ravg)                    |
| 2.  | <b>for</b> ( $R \in Im(:, :, 1)$ ; $G \in Im(:, :, 2)$ ; $B \in Im(:, :, 3)$ ) |
| 3.  | $R_{avg} = Avg(R)$<br>$G_{avg} = Avg(G)$<br>$B_{avg} = Avg(B)$                 |
| 4.  | <b>end</b>   |
| 5.  | <b>Step 2:</b> Compute Gray Value (GV)   |
| 6.  | <b>while</b> ( $Im_{avg} = [R_{avg} \ G_{avg} \ B_{avg}]$ )                    |
| 7.  | <b>do:</b> $GV = sum \frac{Im_{avg}}{size(Im_{avg}, 2)}$                       |
| 8.  | <b>End</b>   |
| 9.  | <b>Step 3:</b> Compute Scale Value (SV)  |
| 10.   | $sv = \frac{GV}{Im_{avg}}$   |
| 11.   | <b>Step 4:</b> White Balanced RGB Components $[R_w \ G_w \ B_w]$               |
| 12.   | <b>while</b> ( $SV \in [sv_R \ sv_G \ sv_B]$ )                                 |
| 13.   | <b>do:</b> $R_w = SV\{1\} * R$<br>$G_w = SV\{2\} * G$<br>$B_w = SV\{3\} * B$   |
| 14.   | <b>end</b>   |

---

In general, natural light only requires correction along the blue-yellow spectrum, but certain types of artificial lighting may produce a noticeable color tint, in which case there is a need to correct for that, too. For the proposed method, the algorithm to construct white balanced image is to first extract the red (r), green (g) and blue(b) components of the input and then white-balance them individually. This is done by extracting the gray values (gv) of the components and then divide the same with the image average (avg). This gives us the scale values (sv). The combined array of the red, green and blue scale values gives the final white-balanced output. The algorithm is summarized as Algorithm 1.

#### 2.4.1.2 Contrast-Enhanced Image

Increasing the difference between the objects in an image and the background leads to contrast enhancement. To perform the same, both the dynamic and static regions of the image need to be addressed. This is done by a two-step approach of tonal adjustment and contrast stretching. Tonal adjustment improves on the specific areas of shadows and highlights, while contrast stretching, increases brightness uniformly. Contrast-Enhancement has been employed in this paper in order to search for any hidden variations in structure or texture in the hazy image.

TABLE X

ALGORITHM 2: ALGORITHM TO CONSTRUCT CONTRAST-ENHANCED IMAGE

---

**Input:** RGB Components of Hazy Image;  $\{Im = [R \ G \ B]\}$

**Output:** Contrast-Enhanced RGB Components;  $\{Im_{ce} = [R_{ce} \ G_{ce} \ B_{ce}]\}$

1. **Step 1:** Compute Luminance (L)
2.     **for** ( $R \in Im(:, :, 1)$ ;  $G \in Im(:, :, 2)$ ;  $B \in Im(:, :, 3)$  )
3.          $L_R = 0.299 \times R$
- $L_G = 0.587 \times G$
- $L_B = 0.114 \times B$
4.     **end**
5. **Step 2:** Determine Colour Balancing Constant (*Gamma*)
6.     **while** ( $L = [L_R \ L_G \ L_B]$ )
7.          $g = 2(0.5 + Avg(L))$  // *Gamma is a constant denoted by g*
8.     **end**
9. **Step 3: Compute Contrast Enhanced RGB components**
10.    **for** ( $R \in Im(:, :, 1)$ ;  $G \in Im(:, :, 2)$ ;  $B \in Im(:, :, 3)$  )
- $R_{ce} = g(R - Avg(L))$
- $G_{ce} = g(G - Avg(L))$
- $B_{ce} = g(B - Avg(L))$
11.    **end**

---

Popular techniques for contrast enhancements include using histogram equalization [25],[26] and CLAHE [30], [31]. If most of the pixels in the image are concentrated in the center of the histogram, then the histogram equalization does help, however if the values are already spread out, using CLAHE would be a better alternative.

Histogram equalization, helps to expose previously hidden features, especially the debris particles on the tire. Unfortunately, at the same time, the enhancement over-saturates several areas of images sometimes making them look washed out. Sometimes, it is better to brighten only certain areas of the image which means that employing different transformations at different areas of the image (CLAHE). For color images, this is typically done by converting the image to a color space that has image luminosity as one of its components.

Contrast adjustment is performed on the luminosity layer only, and then the image is converted back to the RGB color space. Manipulating luminosity affects the intensity of the pixels, while preserving the original colors. This method employs the algorithm presented as Algorithm 2 for contrast enhancement.

#### 2.4.2 Weight Maps

(i) *Weight Map from Gaussian and Steerable Pyramid:*

A Steerable pyramid structure [16] is multi-scale, translation invariant and self-inverting in nature. In other words, it can be used for multiple representations of the same image and the coefficients obtained in between the process, are of the same size as the original image.

This is because the projections of the steerable filters and that of the basis functions are identical [17]. The image is first filtered through steerable kernels. Kernels are matrices that are concatenated to form filters (Figure 5). The image is thus split into a highpass component and other residuals. The residuals are passed through the next steerable kernel to obtain lower passbands and subbands oriented in different projections in space. The subbands are called basis functions and recursive splitting of the lower passband, forms the rest of the pyramid. The property of steerability in the kernels gives the ability of orientation tuning however, the recursion technique employed to build the pyramid, constraints scale tuning ability. To overcome this issue, frequency domain construction [18] is preferred and has been employed for this work. The property of steerability in the kernels gives the ability of orientation tuning however, the recursion technique employed to build the pyramid, constraints scale tuning ability. To overcome this issue, frequency domain construction [18] is preferred and has been employed for this work.

In this work, the fourth sub band matrix has been transmitted via the gaussian pyramid to create the corresponding weight map called a steer-gauss map. Since this weight map has been directly derived from the hazy input image, it aids in filling in information gaps during the formation of the final dehazed image.

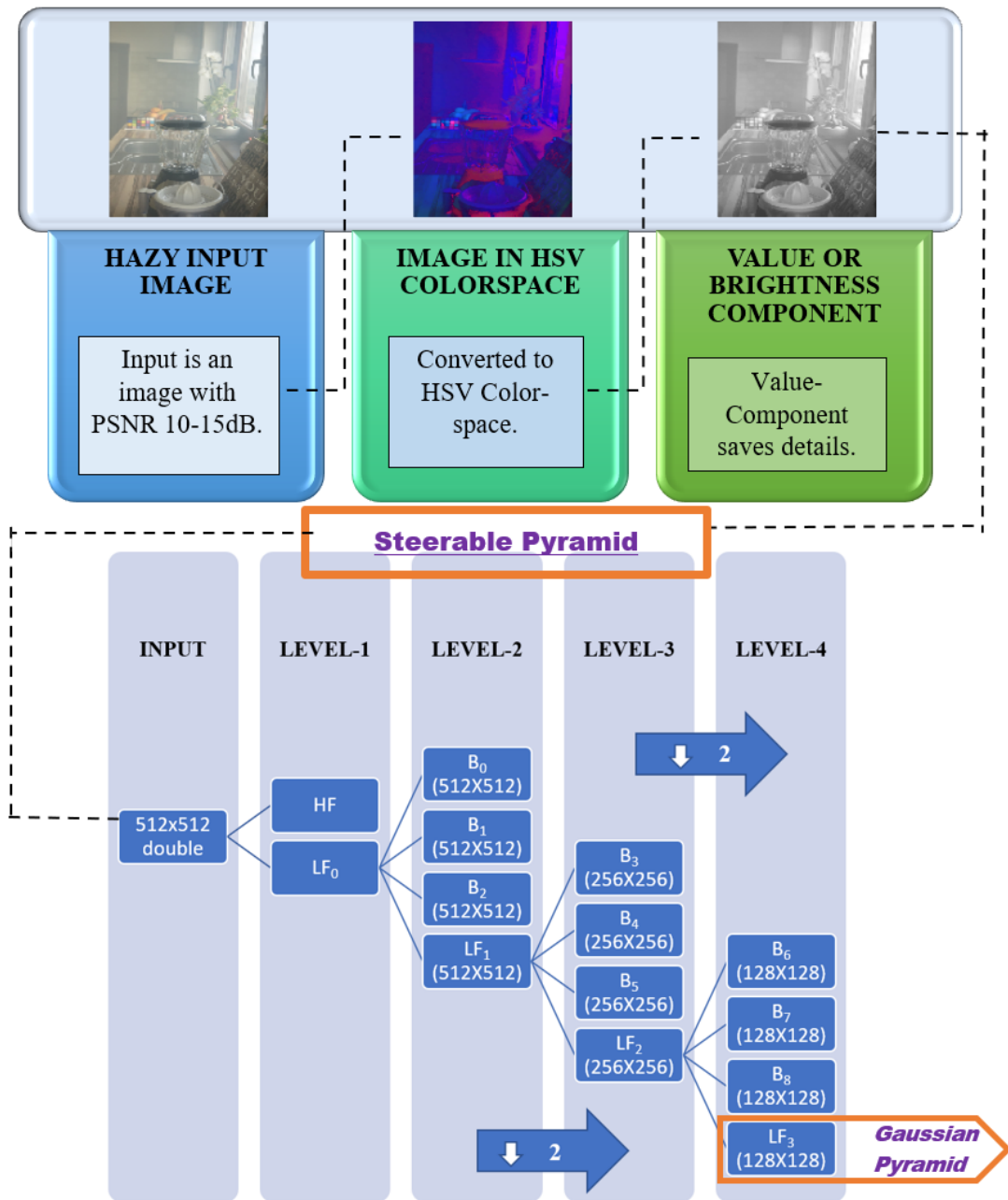


Figure 5-Weight Maps

(ii) Weight maps from derived inputs:

The Laplacian pyramid is used to process the derived inputs to get contrast-enhanced and white-balanced weight maps (Figure 6). The Laplacian pyramid becomes an essential part of the process.

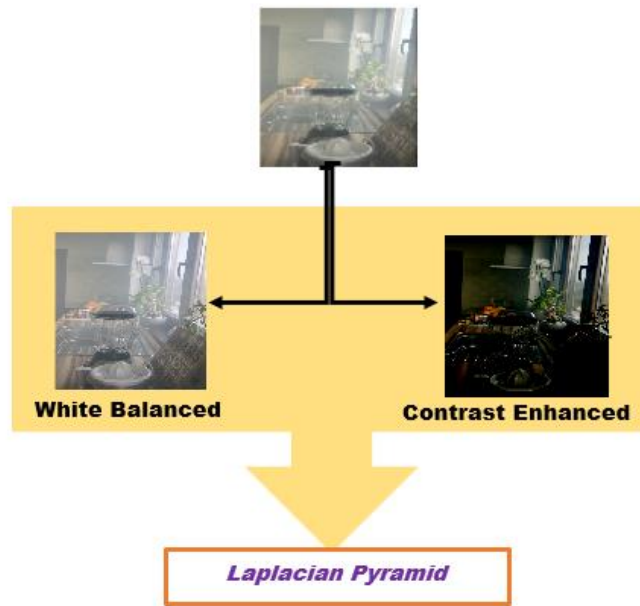


Figure 6-Weight Maps from derived inputs

Passing through the Laplacian pyramid sharpens the image by re-discovering hidden edges of the object without disturbing white balance or contrast. This excellent method has also been employed by Ancuti et al. [1] and has been reused as a part of the proposed method.

#### 2.4.3 Multi-Scale Fusion

The fusion operation is performed by pixel-wise multiplication of the weight maps obtained as a result of the Gaussian and Laplacian pyramids. An important point to note is that the decomposition level or the number of layers for both the Laplacian and Gaussian pyramids must be the same for proper fusion. Also, the weight maps which are to be fused must remain at the same sizes. Successively, the multiplication operation in a bottom-up manner combines the different weight maps derived during processing [1]. The last step is to sum the final outputs of all the layers to create the dehazed image.



## CHAPTER 3

### PROPOSAL-2

#### 3. A RETINEX PRIOR TO MULTI-SCALE FUSION FOR SINGLE IMAGE DEHAZING

This experiment proposes to extract reflectance matrices and incorporate them into the multi-scale fusion algorithm. The technique proposed aims to reduce the halo effect observed in image-dehazing applications and related works for heavily hazy images. Moreover, an improvement in the quality of the output using the proposed novel algorithm is observed. Quantitative, as well as a visual display of results, using the DENSE HAZE dataset, give an accurate interpretation of the effectiveness of the proposed work.

##### 3.1 Introduction

Images captured in presence of atmospheric haze show a layer of blurring in the final output. Digital cameras have multiple filters that can compensate for the lighting conditions in a captured image by changing the tonal quality of the image. However, the layer of haze hides the actual structure of the object and thus, no amount of cleaning compensates for the lack of information in the image. Therefore, hazy regions of an image can be considered lost information. To compensate for the lost image quality and clarity, many methods have been researched. The review paper [112], lists the methods employed for image dehazing over the past few years. Broadly, related methods can be classified as learning-based and non-learning-based. The learning-based methods employ techniques ranging from transfer learning approaches [2-6], to complex deep-learning networks [7-15], for depth-map estimations. The non-learning-based methods include Image Enhancement, Image restoration-degradation and Image Fusion based techniques.

Image Enhancement generally comprises methods aimed at improving the input hazy image to generate its clearer counterpart. This method is preferable when ground truth is not present. The model most common to literature employed to support this methodology is the Atmospheric-Scattering model where the degradation associated with haze has been attributed to a combination of transmission loss and airlight. The transmission map or depth map for a hazy image can be computed using a variety of methods and is the solution to reconstructing a haze-free image. Subdomains under Image Enhancement techniques are histogram processing [16-20] and the Retinex method [21-25]. In case there is the availability of the ground truth image, the Restoration-Degradation model of Image dehazing is preferred. In this technique, the type and quantity of degradation afflicted on the image are computed as a first step by the researcher. This is done by comparative analysis of the ground truth and hazy

image. The second step is called image restoration and is based on the information obtained by the researcher in the first part of the technique, degradation. The restoration methods are thus based on the degradations performed on the image and hence, a variety of methodologies can be observed in the literature [26-30]. The third category is Fusion-based Image dehazing techniques. The main principle behind Fusion-based techniques is the iterative multiplication of weight maps derived from one (Single-Scale) or multiple (multi-Scale) versions of the parent hazy image. The derivations of weight maps thus become a central research area. Though the procedure seems to be easy at a glance, the haze-free reconstruction version of the input image is a perfect balance of contrast, hue, luminance and other parameters. The major issues plaguing the fused images are the halo effect, low visibility around edges, lack of similarity to the ground truth etc. This paper proposes Image dehazing by combining the Retinex method and Image Fusion technology. The choice of the Retinex method is supported by the fact that the output of the Retinex method mimics human vision and gives a good representation of the hazy image and its features. The image extracted as the reflectance component from the hazy image is transmitted via a Gaussian Pyramid algorithm [113] to allow inpainting (gap filling). The inpainting operation is basically a technique to compensate the blur-inflicted regions of the hazy image with information. The ‘information’ here is the pixel content which gets blurred in hazy images and the proposed method helps in retrieving this pixel information by simultaneously computing the reflectance component from the ground truth of the hazy image. The outputs of the Gaussian pyramid are the weight maps for image fusion. Inspired by the fusion strategy employed by Ancuti et al. [37], the reflectance maps are also passed via the Laplace Pyramid algorithm [113] to generate edge-sensitive information from the hazy image. Finally, the four weight maps are fused to obtain a dehazed result. This work takes inspiration also from Jobson et al. In their paper [114], they explore the Retinex algorithm for processing colour images. They suggest employing the retinex method by using the Hue-Saturation\_Value (HSV) version of the image and then reconvert it into Red-Green-Blue (RGB). This method retains the matrix compatibility with the Retinex algorithm and also preserves the colour of the image. The present paper suggests using the HSV components of the image to dehaze it using the above-proposed methodology and as a last step, perform colour restoration using an algorithm inspired by Jobson et al. [114]. The major objective that the paper aims to achieve is to develop a novel methodology to dehaze heavily hazy images by using the Image-Fusion strategy. The proposed method proves to be advantageous in the sense that it is low in complexity, requires less computation time and is able to dehaze images that are 60-70% blurred in the image area. The star of the show is the simultaneous use of both the hazy and ground truth’s reflectance maps while performing fusion. The reflectance map of ground truth proves to be essential in computing lost pixel intensities of hazy regions. The Retinex method by itself is not the best method for dehazing and needs preprocessing to create good-quality outputs. The use of Gaussian and Laplacian pyramids proves to be the required bridge for fusion and the generated depth maps. The proposed method has been compared against the results obtained by related works of Ancuti et al. [37], Jobson et al. [114] and Dalvi et al. [115]. Quantitative parameters like Structural

Similarity Index (SSIM), Peak Signal-to-Noise Ratio (PSNR), etc. for the proposed work are also computed and compared with related works. The dataset used for validation is the DENSE-HAZE dataset used in the CVPR NITRE competition of 2019 [116] comprising fifty-five hazy and ground truth images. The paper develops a novel strategy to create a novel algorithm for image dehazing that combines the Retinex and Multi-Scale Fusion methodologies to generate colored dehazed images.

### 3.2 Background Theory

The proposed method employs the Retinex algorithm to compute the reflectance of the image. The Retinex algorithm states that pixel intensity of an image ( $I$ ) is the product of Illumination ( $IL$ ) and Reflectance Ratio ( $RR$ );

$$I = IL \times RR \quad (12)$$

The Reflectance can thus be calculated by the following steps;

$$\log(I) = \log(IL) + \log(RR) \quad (13)$$

$$RR = 10^{\log(I) - \log(IL)} \quad (14)$$

The above steps do not support preserving the color component of the input image. The multi-scale Retinex algorithm [114] is employed to calculate the reflectance with the color of the image. The present method proposes to incorporate the obtained reflectance into the gaussian and laplacian pyramid algorithms to generate corresponding weight maps which act as a substitute for the transmission map of the hazy input image. These maps are then fused to obtain the final dehazed results.

### 3.3 Multi-Scale Retinex based Fusion Methodology

#### 3.3.1 Multi-Scale Retinex

Lightness perception is the perception of achromatic surface colors of black, white, and shades of grey. In other words, it is perceived reflectance. The principle finding of Retinex theory for human visual system is that the eyes perceive variations in lightness in the local regions of the image. To incorporate the variability, the Retinex method averages the lightness obtained from different paths, where, each path starts at random points of the image and end at a pixel. The Multi-Scale Retinex assumes the weighted average of many Single-Scale Retinex's outputs as its final output. From equation (14) it is observed that there need to be some constant parameters to smoothen the transformation of the output from logarithmic to linear domain for visualization. The method proposed by Jobson et al. [114], attempts to find a solution. In their paper, it is observed that there is a particular gaussian shape of the Retinex output histogram with large tails extending on both sides. To obtain good contrast, the extreme tails need to be clipped off. Jobson calls the process "canonical gain/offset", however does not specify values to compute this. To counter the issue, the paper by Petro et al. [117], proposes to use Simplest Color Balance algorithm which stretches the Red, Green and Blue (RGB) component to the maximum value [0,255] clipping some percentage of pixel on either side. This algorithm they coin as Multi-Scale Retinex with color Restoration (MSRCR) and use 1% clipping on both

sides in their paper. For the proposed algorithm, 5% clipping from both sides has been performed.

In the Proposed algorithm, both the Hazy and its clear counterpart-Ground Truth (GT) images are required. First step is to compute the maximum channel in the image as an approximation of the image illumination. Next is the computation of the reflectance components from the obtained illumination using the Multi-Scale Retinex algorithm with the appropriate “scale” array (it should have 3 values corresponding to each weight according to Jobson et al.). To preserve the color component of the picture, first convert the Hazy image and GT to their HSV format. On replacing the Value component with the obtained Retinex output (Reflectance), we obtain the preliminary Retinex weight maps.

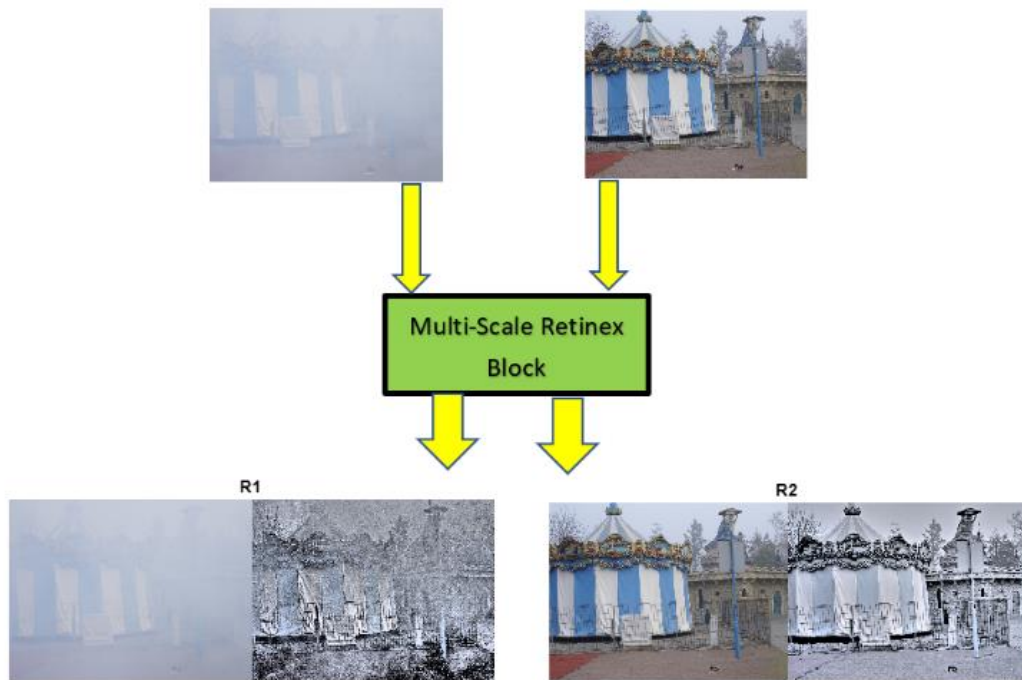


Figure 7-Retinex Weight Maps

### 3.3.2 Normalized Weight Maps

The preliminary components thus achieved, are both once passed through the Gaussian and once through the Laplacian pyramids to generate corresponding weight maps for both the hazy and GT images. The decomposition level of five has been taken for the Laplacian and Gaussian pyramids.

### 3.3.3 Multi-Scale Fusion

Each level of the 5-level Gaussian decomposition is individually multiplied by the corresponding Laplacian level to create an iterative product network of intermediate images. The product outputs are then added to create a fusion image which is the superposition of all intermediate matrices (Figure 7). Due to the presence of reflectance information from both the hazy and GT images, any pixel gaps are inpainted. Thus, the enhanced image is obtained.

### 3.3.4 Color Restoration

The end step of the Multi-Scale Retinex-based Fusion methodology is the restoration of the color component that was lost to the Retinex algorithm. Basically, due to the addition of the “lightness template”, the overall image gets faded and seems devoid of its colors. One of the methods devised was to extract the color map of the GT and then use the information to reinstall color in the dehazed output. However, such a method always poses the risk of an uneven color gradient distribution. Hence, the color map restoration has been performed based on color balancing. The technique of color balancing computes a 2-dimensional matrix which is the difference between the mean of the enhanced image and the product of dynamic range and variance of the enhanced image. Since the variance and mean calculations are subject of the enhanced image, no padding is necessary for the computations, thereby eliminating the risk of uneven pixel maps.

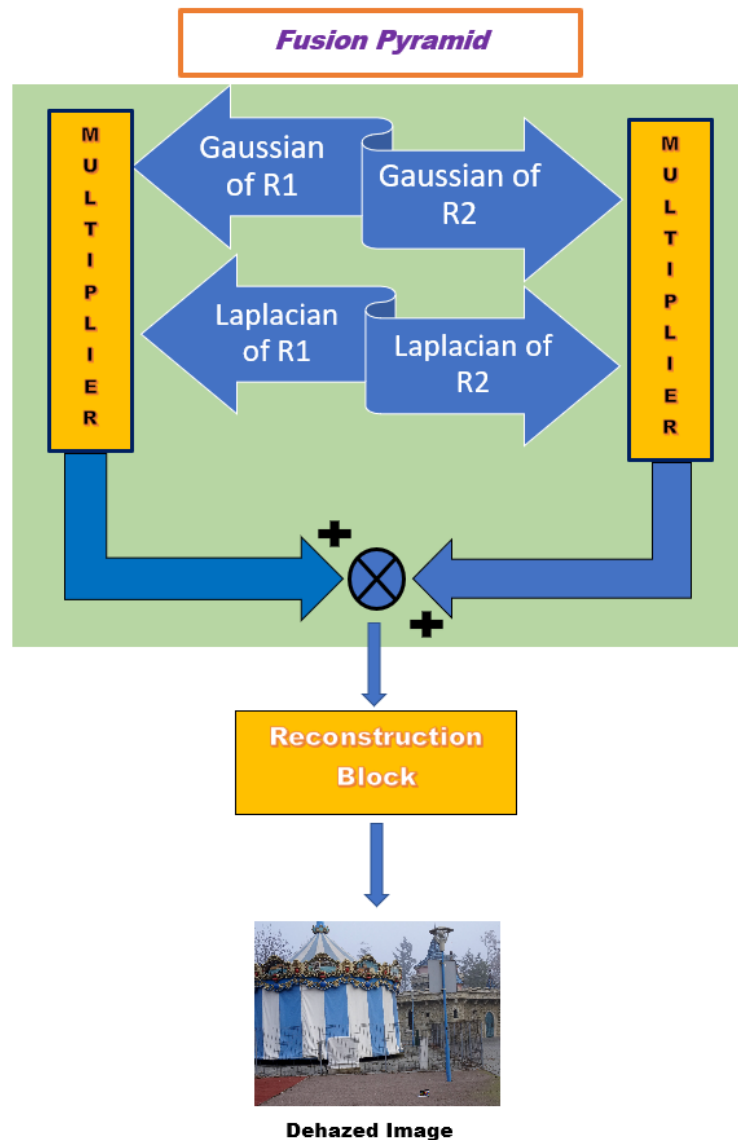


Figure 8-Fusion Pyramid

## CHAPTER 4

### RESULTS AND DISCUSSION

#### 4. IMAGE DEHAZING AND FUSION PYRAMIDS

The major objective of this dissertation is to establish an image dehazing approach that sharpens the image by re-discovering hidden edges of the object without disturbing white balance or contrast for color images. Saliently, the proposals presented steer away from complicated methods like deep learning to achieve a depth-aware framework for effective haze-removal.

##### 4.1 Statement Analysis

The following section elaborates on the conclusive evidence in support of the final technique adopted and states the proceedings for its implementation.

##### 4.1.1 Why Fusion-based Image Dehazing?

The vast research on Image dehazing can be categorized based on the dehazing techniques employed by the researchers in popular literature. The flow chart of Figure 2 gives a brief idea about the different image dehazing approaches. Under the aegis of image dehazing by Image Enhancement, the research area mainly focuses on improving the view of hidden objects in the image by equalizing its contrast. Popular methods include Histogram Equalization, CLAHE, Retinex. The next category of Image Dehazing is dehazing by Image Restoration, which is different from Image Enhancement, because the latter does not require the researcher to know the exact degradations plaguing the image. Image Restoration in its fullest sense is a method that aims at re-doing or inverting the degradations performed on the image, that made it blurry in the first place. In a general sense, the Image Restoration method for Image Dehazing is a Restoration-Degradation model. DCP is one of the examples. Image Restoration, however, mandates the use of a transmission map or depth map or image prior for image dehazing. Image Enhancement offers a significant advantage in this sense but, it is not efficient in case there are multiple images of the same scene or object just like in the case of the databases of Geographic Interphase System (GIS), where, there is a vast array of images of the same area from different angles and depth. Image Fusion then takes the lead because the method works by inculcating features from all available images of the scene/object under surveillance. Furthermore, in instances where images of a ‘moving’ object, like a human lung, growing cancer tumour, etc., are recorded, image fusion becomes necessary to combine all geometric transformations of the object to form a single master image.

### 4.1.2 Pyramidal Structure

So far, the superiority of Image Fusion technique for our major objective has been established. Fusion-based techniques generally follow a pyramidal approach. If illustrated graphically, the entire multi-scale representation will look like a pyramid, with the original image on the bottom and each cycle's resulting smaller image stacked one atop the other. Both the proposed ideas employ two types of pyramids, the Gaussian Pyramid which is essentially a lowpass pyramid and the Laplacian pyramid which uses a bandpass kernel. Since the gaussian pyramid helps in removing unwanted aliasing and the Laplacian pyramid enables computation of pixelwise differences; both have been performed for the proposed technique.

### 4.1.3 Weight Maps

Weight maps provide a depth-aware expression of the input image. The choice of weight maps stems from the reference papers [37], [115] where the use of White-balanced and Contrast-Enhanced counterparts of the image as weight maps was suggested. The area of image dehazing has many such examples in this domain however, the use of weight maps has its own disadvantages. It is impossible to use an infinite number of weight maps to extract each feature. Considering the specific weight maps used in proposal 1, there is no way to know how much white-balancing and contrast enhancement is appropriate for an image since each image has different degree of haze. Hence there is no way to generalize the process. On applying the proposed method on images having a greater haze (PSNR < 10 dB), the technique fails to remove haze.

The countermeasure was to use Retinex based weight maps. The principle finding of Retinex theory for human visual system is that the eyes perceive variations in lightness in the local regions of the image. To incorporate the variability, the Retinex method averages the lightness obtained from different paths, where each path starts at random points of the image and end at a pixel. The use of Retinex weight maps generalizes the technique along with giving a depth-aware map for dehazing.

### 4.1.4 Multi-Scale Fusion

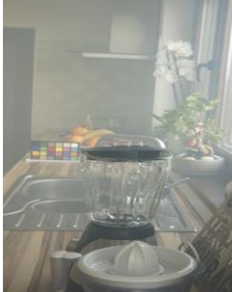


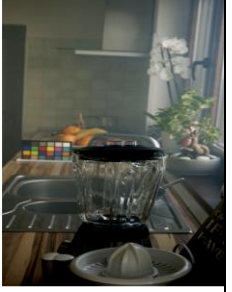
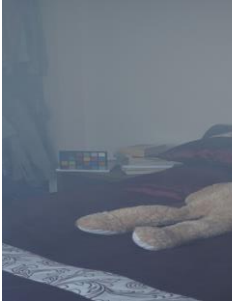


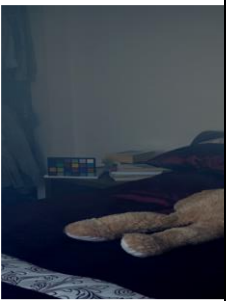






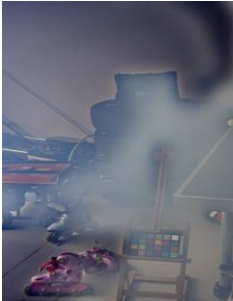

The multi-scale fusion technique enables the use the details that are obtained as a result of converting the image to some other scale, which were not visible earlier. The fusion operation is performed by pixel-wise multiplication of the weight maps obtained as a result of the Gaussian and Laplacian pyramids. Due to the presence of reflectance information from both the hazy and GT images, any pixel gaps are in-painted. Thus, the enhanced image is obtained. In-painting is a technique to fill-in the missing gaps of information in the image, the main problem that arises in the use of this technique is the decrease of resolution in the image. However, with the use of Retinex, the resolution seems to be maintained and enhanced according to the no-reference quantitative values obtained.

## 4.2 Qualitative Results

The significant difference between Ancuti et al [37], Dalvi et al. [115] and the proposed work is the use of a lowpass coefficient matrix of the original image. The coefficient matrices are derived from the steerable pyramid and are then fed to the gaussian pyramid as input. The visual results are compared with related works [37], [115] using the I-HAZE [103] dataset for validation. This paper

presents the dehazed results of four images from [103] namely, Teapot (I-HAZE:09), Teddy (I-HAZE:19), Telescope (I-HAZE:01) and Playroom (I-HAZE:35). The Steerable pyramid employed in this paper decomposes the image into 5 levels using one high and four low pass filters. It is observed that the proposed work is independent of the level of decomposition selected [113].

**TABLE XI**  
**RESULTS FOR PROPOSAL 1**


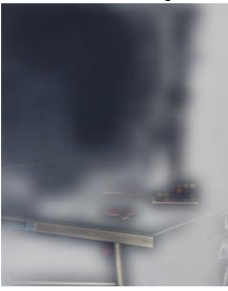

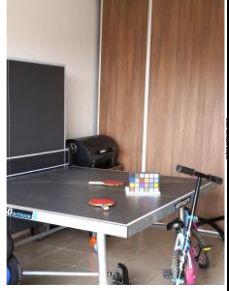





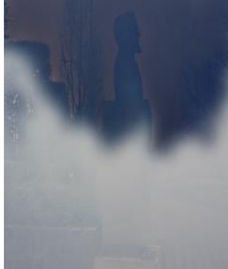
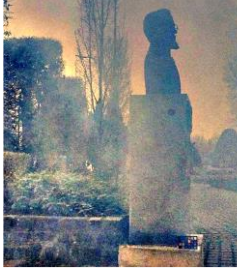
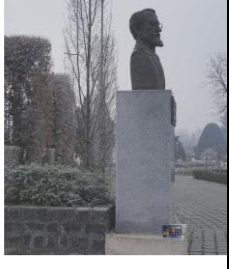




| <i>Image</i>    | <i>Hazy Input Image</i>   | <i>Ancuti et al</i>   | <i>Dalvi et al.</i>  | <i>Proposed Method</i>  |
|-----------------|---|---|--|---|
| Tea-<br>pot     |    |    |    |    |
| Teddy           |   |   |   |   |
| Tele -<br>scope |  |  |  |  |
| Play-<br>room   |  |  |  |  |

Hence, based on visual observations, the fourth level of decomposition has been selected for this work. Some major regions of notice are the images' background and the picture's bottom. In the dehazed image presented in Table XI, it is noticed that no information has been lost to dehazing and the background and foreground are clearly visible unlike the results of both methods. Moreover, the halo



effect is significantly reduced in the background which is a major problem in Telescope and Playroom Images. The results are compared and tabulated in Table XI.

**TABLE XIII**  
**RESULTS FOR PROPOSAL 2**

| <i>Image</i> | <i>Hazy Input Image</i>   | <i>Dalvi et al.</i>   | <i>Jobson et al.</i>   | <i>Proposed Method</i>  |
|--------------|---|---|--|---|
| Table Tennis |    |    |    |    |
| Park         |   |   |   |   |
| Bust         |  |  |  |  |
| Castle       |  |  |  |  |

The proposal 2 has been validated on the DENSE-HAZE dataset comprising fifty-five densely hazed images and their ground truths. The visual results are compared with a few related works in literature; an improvement to the the Multi-Scale based Fusion technique by Ancuti et al. [32] by Dalvi et al. [34] and the reference paper for the Multi-Scale Retinex algorithm by Jobson et al. [33]. The visual results for the TT playroom (Image 55 of [35]) are summarized in Table XII. From the table, it is clear that the dense haze creates many hurdles for the method proposed by Ancuti et al. [32] because the underlying principle of feature enhancement fails to make a suitable distinction between haze and background. Similarly, the results observed for the method by Dalvi et al. [34] creates a big halo in

TABLE XIII

QUANTITATIVE ANALYSIS OF THE PROPOSED METHOD VERSUS THE RESULTS OF ANCUTI ET AL.

| <i>Images</i>    | <i>Ancuti et al.</i> |       |      |      |         | <i>Proposed Method</i> |       |      |      |         |
|------------------|----------------------|-------|------|------|---------|------------------------|-------|------|------|---------|
|                  | SSIM                 | PSNR  | MSE  | NIQE | BRISQUE | SSIM                   | PSNR  | MSE  | NIQE | BRISQUE |
| <b>Teapot</b>    | 0.36                 | 9.976 | 0.10 | 3.10 | 28.1294 | 0.36                   | 10.26 | 0.09 | 2.90 | 18.8559 |
| <b>Teddy</b>     | 0.52                 | 11.47 | 0.07 | 3.94 | 31.4826 | 0.56                   | 13.09 | 0.04 | 3.34 | 22.8193 |
| <b>Telescope</b> | 0.49                 | 10.05 | 0.09 | 3.08 | 30.7487 | 0.41                   | 9.706 | 0.10 | 3.05 | 20.1761 |
| <b>Playroom</b>  | 0.56                 | 10.71 | 0.08 | 3.77 | 38.9794 | 0.55                   | 11.05 | 0.07 | 3.35 | 30.7017 |

TABLE XIV

QUANTITATIVE ANALYSIS OF THE PROPOSED METHOD VERSUS THE RESULTS OF DALVI ET AL.

| <i>Images</i>    | <i>Dalvi et al.</i> |       |      |      |         | <i>Proposed Method</i> |       |        |      |         |
|------------------|---------------------|-------|------|------|---------|------------------------|-------|--------|------|---------|
|                  | SSIM                | PSNR  | MSE  | NIQE | BRISQUE | SSIM                   | PSNR  | MSE    | NIQE | BRISQUE |
| <b>Teapot</b>    | 0.49                | 13.32 | 0.04 | 3.15 | 26.3851 | 0.36                   | 10.26 | 0.09   | 2.90 | 18.8559 |
| <b>Teddy</b>     | 0.65                | 14.00 | 0.03 | 4.37 | 33.1575 | 0.56                   | 13.09 | 0.0491 | 3.34 | 22.8193 |
| <b>Telescope</b> | 0.49                | 7.699 | 0.16 | 3.48 | 33.3251 | 0.45                   | 9.706 | 0.1070 | 3.05 | 20.1761 |
| <b>Playroom</b>  | 0.65                | 13.32 | 0.04 | 3.67 | 39.8957 | 0.55                   | 11.05 | 0.07   | 3.35 | 30.7017 |

place of the haze in the original image. The Multi-Scale Retinex method proves to be much better but the pixel distribution in the dehazed image is not proper and uniform. The proposed method shows better clarity and is visually better than the other outputs.

The visual results show

- Marked improvement in colour contrast.
- Absence of Halo effects
- Clearer edge boundaries
- No Compression/pixel distortion.

### 4.3 Quantitative Results

Some other parameters like SSIM, PSNR etc. are summarized in Table XII and XIII. In Table XII, the SSIM [19] for the proposed work does not vary significantly from the related work. Since the haze has been removed, the values of SSIM are quite low for both images. The improvement in PSNR [20] values indicate good quality result, with the exception being the Telescope image, as seen in the third row of Table XII. Likewise, MSE [21] values are compared for both methods and expectedly, the Telescope image proves to be an exception. A reduction in MSE values is observed in the results of the proposal as compared to traditional methods. The performance metrics computed before are with the original hazy image taken as a reference. Two other parameters have been listed to encompass the non-reference image quality metrics, NIQE [22] and BRISQUE [23]. On comparing the proposed method with that devised by Dalvi et al., all the images show a decrease in SSIM values. The good SSIM value can be credited to the excellent method proposed by them. Moreover, it is observed the

TABLE XV

QUANTITATIVE ANALYSIS OF THE PROPOSED METHOD VERSUS THE RESULTS OF ANCUTI ET AL.

| <i>Images</i> | <i>Ancuti et al.</i> |       |      |      |         | <i>Proposed Method</i> |       |        |      |         |
|---------------|----------------------|-------|------|------|---------|------------------------|-------|--------|------|---------|
|               | SSIM                 | PSNR  | MSE  | NIQE | BRISQUE | SSIM                   | PSNR  | MSE    | NIQE | BRISQUE |
| <b>TT</b>     | 0.38                 | 4.965 | 0.31 | 4.6  | 43.1362 | 0.91                   | 16.25 | 0.0237 | 2.62 | 25.2310 |
| <b>Park</b>   | 0.34                 | 7.054 | 0.19 | 3.72 | 24.0035 | 0.04                   | 8.996 | 0.2226 | 2.69 | 39.2781 |
| <b>Bust</b>   | 0.29                 | 6.109 | 0.25 | 2.60 | 20.7554 | 0.04                   | 9.878 | 0.1028 | 3.21 | 23.8942 |
| <b>Castle</b> | 0.33                 | 5.188 | 0.30 | 2.74 | 20.5156 | -0.05                  | 10.05 | 0.0988 | 2.57 | 9.1978  |

TABLE XVI

QUANTITATIVE ANALYSIS OF THE PROPOSED METHOD VERSUS THE RESULTS OF DALVI ET AL.

| <i>Images</i> | <i>Dalvi et al.</i> |       |      |      |         | <i>Proposed Method</i> |       |        |      |         |
|---------------|---------------------|-------|------|------|---------|------------------------|-------|--------|------|---------|
|               | SSIM                | PSNR  | MSE  | NIQE | BRISQUE | SSIM                   | PSNR  | MSE    | NIQE | BRISQUE |
| <b>TT</b>     | 0.64                | 8.479 | 0.14 | 5.72 | 57.1662 | 0.91                   | 16.25 | 0.0237 | 2.62 | 25.2310 |
| <b>Park</b>   | 0.44                | 12.28 | 0.05 | 4.03 | 23.0836 | 0.04                   | 8.996 | 0.2226 | 2.69 | 39.2781 |
| <b>Bust</b>   | 0.47                | 14.77 | 0.03 | 3.60 | 26.1566 | 0.04                   | 9.878 | 0.1028 | 3.21 | 23.8942 |
| <b>Castle</b> | 0.55                | 9.513 | 0.11 | 3.67 | 26.2794 | -0.05                  | 10.05 | 0.0988 | 2.57 | 9.1978  |

TABLE XVI

QUANTITATIVE ANALYSIS OF THE PROPOSED METHOD VERSUS THE RESULTS OF JOBSON ET AL.

| <i>Images</i> | <i>Jobson et al.</i> |       |      |      |         | <i>Proposed Method</i> |       |        |      |         |
|---------------|----------------------|-------|------|------|---------|------------------------|-------|--------|------|---------|
|               | SSIM                 | PSNR  | MSE  | NIQE | BRISQUE | SSIM                   | PSNR  | MSE    | NIQE | BRISQUE |
| <b>TT</b>     | 0.01                 | -9.94 | 9.88 | 11.8 | 43.7758 | 0.91                   | 16.2  | 0.0237 | 2.62 | 25.2310 |
| <b>Park</b>   | 0.00                 | -8.45 | 7.00 | 16.0 | 44.4770 | 0.04                   | 8.996 | 0.2226 | 2.69 | 39.2781 |
| <b>Bust</b>   | 0.01                 | -6.14 | 4.11 | 15.0 | 44.0125 | 0.04                   | 9.878 | 0.1028 | 3.21 | 23.8942 |
| <b>Castle</b> | -0.01                | -8.07 | 6.41 | 12.3 | 53.3519 | -0.05                  | 10.05 | 0.0988 | 2.57 | 9.1978  |

proposed method shows improvement neither in the PSNR values nor in the error estimates by the MSE method except for the case of the Telescope image. In spite of the poor performance, the visual results are better for the proposed method as compared to Dalvi and this fact is proved by the significant reduction in values of NIQE and BRISQUE techniques for all images used in validation.

Table XV provides a few measures for quantitative analysis of the second proposal and other related works. The images selected from the dataset [35] are TT Playroom (Image no. 55), Park (Image no. 01), Bust (Image no. 07) and Castle (Image no. 47). The best value of Structural Similarity Index (SSIM) obtained is 0.9128 which shows a 62% increase in image quality as compared to average SSIM values of previously known methods. The Peak Signal to Noise Ratio (PSNR) and Mean Square Error (MSE) show improvement by 78% (TT Playroom) and 95% (Castle) respectively.

To allow analysis with regards to pixel compression that may have resulted during the process, two No Reference Image Quality Metrics have been also computed. The Naturalness Image Quality Evaluator (NIQE) compares the input to a default image. A small value indicates better image quality. Blind/Referenceless Image Spatial Quality Evaluator (BRISQUE) does not even use a default image.

All features for detecting quality are derived from the input image itself. Just like NIQE, a lower BRISQUE indicates a better image quality. On comparing the results of NIQE with the methods of Dalvi and Ancuti et al, there is not much improvement, however, there is significant improvement observed on comparing the method with Jobson et al. BRISQUE results are much more promising and shows improvement with all three methods computed.

## CHAPTER 5

### CONCLUSION

#### 5. FUSION BASED TECHNIQUES FOR SINGLE IMAGE DEHAZING

##### 5.1 Motivation

The existing methods for Image Dehazing by fusion are subdivided into two broad fields-using fusion pyramids and using deep learning networks to process the depth maps of the input image. It is evident that the methods incorporating Deep Learning algorithms have gained popularity amongst the researchers due to their reliability in estimating the depth maps, however making the process very complex. Moreover, these methods show a dependence on large training data for ‘learning’. Nevertheless, research for the fusion pyramid-based approach has been pending. Hence, this dissertation is an attempt to find a suitable approach to single image dehazing using fusion-pyramids.

##### 5.2 Statement Analysis

Steerable Pyramid-based Multi-Scale Fusion algorithm for Single Image Dehazing is a method that uses Steerable pyramid at its core. The weight maps resulting from contrast-enhancement and white balancing are employed. The output from the steerable pyramid is fed to Gaussian pyramid and the weight maps are passed via Laplacian pyramid. Finally, the results are multiplied pixel-wise, and the intermediate results are added to generate a fused-output. The same is reconstructed to generate dehazed image.

A Retinex prior to Multi-Scale Fusion for Single Image Dehazing is an advancement to proposal 1 and employs Multi-Scale Retinex to generate depth-maps from hazy image and its GT. Both are then passed via Laplacian and Gaussian pyramids to generate corresponding templates. The same process of pixel-wise multiplication followed by reconstruction is used to generate dehazed output.

##### 5.3 Outline

The major similarities and differences between the proposed algorithm with the existing works in literature are presented below:

- (i) Main Idea:
- (ii) Techniques used:
- (iii) Results Obtained:

##### 5.4 Significance

Dehazing is vital for many computer-vision algorithms used in remote sensing, agricultural monitoring, intelligent vehicles, object recognition, and surveillance that assume the hazy image as original scene radiance and hence suffer from bias. The

work presented in this thesis provides two suitable algorithms to dehaze indoor and outdoor hazy images respectively so as to promote better applicability.

### **5.5 Conclusion**

The Dissertation encompasses a review of the different means and techniques of image dehazing followed by novel strategies to dehaze indoor and outdoor environmental images. In the first proposed algorithm Steerable Pyramid-based Multi-Scale Fusion algorithm for Single Image Dehazing, a new Multi-scale, Multi-pyramid Fusion based strategy has been proposed for image dehazing. The method employs a Steerable Pyramid to extract information from the low frequency sub-band of the input image and discards the noisy high-frequency band. This method aids in saving vital information to reconstruct the dehazed image. The use of the Laplacian pyramid has been retained from previous related works to transfer the edges identified. Moreover, the fusion strategy in the proposed work, uses the method of products to retain all information. The steerable coefficient matrices prevent hallow formation in the background and retains the colors of the foreground. The proposed method has been validated by the images from dataset I-HAZE and the performance metrics SSIM, PSNR, NIQE, etc. have been extracted. The visual and quantitative results show the superiority of the algorithm presented. However, the method fails for outdoor haze. The second proposal, A Retinex prior to Multi-Scale Fusion for Single Image Dehazing explores Image Dehazing by using Multi-Scale Retinex-based Fusion methodology. This method first studies the Retinex algorithm and concludes from literature that it shows remarkable performance for gray scale images but does not fit well with color images. Another algorithm that the method employs is the multi-scale fusion based dehazing algorithms in common parlance. The main objective of the paper is to formulate an image dehazing framework that eliminates the drawbacks of existing Retinex algorithms by combining Fusion based Dehazing with Multi-Scale based Retinex algorithms. The proposed method has been validated by the images from DENSE HAZE dataset and the performance metrics SSIM, PSNR, NIQE, etc. have been extracted. The visual and quantitative results show the superiority of the algorithm presented.

## REFERENCES

- [1] M. N. Shruti P. Patel, "A review on methods of image dehazing," *International journal of computer applications*, vol. 113, no. January, 2016.
- [2] X. Y. Wencheng Wang, "Recent Advances in Image dehazing," *IEEE/CAA Journal of Automatica Sinica*, vol. 4, pp. 410-436, 2017.
- [3] V. K. Dilbag Singh, "A comprehensive review of computational dehazing techniques," *Springer: Archives of computational Methods in engineering*, pp. 1395-1413, 2018.
- [4] S. Y. J.-H. N. C. S. W. & S.-W. J. Sungmin Lee, "A review on dark channel prior based image dehazing algorithm," *Springer: EURASIP journal on image and video processing*, 2016.
- [5] World Meteorological Organization, "'WMO Manual on Codes" (PDF)," Wikipedia the free encyclopedia, [Online]. Available: <https://old.wmo.int/extranet/>.
- [6] Wikipedia, "Haze (Optic)," Wikipedia the free encyclopedia, [Online]. Available: [https://en.wikipedia.org/wiki/Haze\\_\(optics\)](https://en.wikipedia.org/wiki/Haze_(optics)).
- [7] M. M. A. F. S. e. a. Asmala Ahmad, "Haze Effects on Satellite Remote Sensing Imagery and their Corrections," (*IJACSA*) *International Journal of Advanced Computer Science and Applications*, vol. 10, no. 10, 2019.
- [8] T. A. K. R. R. M. P. P. Thiruvikraman, "A Survey on Haze Removal Techniques in Satellite Images," *rish Interdisciplinary Journal of Science & Research (IJISR)*, vol. 5, no. 2, pp. 01-06, 2021.
- [9] Wkipedia, "Mist," Wikipedia the free encyclopedia, [Online]. Available: <https://en.wikipedia.org/wiki/Mist>.
- [10] M. R. J. Bejgier, "Parallel Simulation of Atmospheric Halo Phenomena.," in *Chmielewski, L.J., Kozera, R., Shin, BS., Wojciechowski, K. (eds) Computer Vision and Graphics. ICCVG. Lecture Notes in Computer Science, vol 8671.*, Springer, 2014.
- [11] NASA's Deep Dive Planetary website, *Saturn*, NASA.
- [12] Wkipedia, "Underwater vision," Wkipedia the free encyclopedia, [Online]. Available: [https://en.wikipedia.org/wiki/Underwater\\_vision](https://en.wikipedia.org/wiki/Underwater_vision).
- [13] E. W. M. Born, "Refraction and Reflection at a metal surface," in *Principles of Optics*, Pergamon Press Ltd., 1986.
- [14] Hecht, "Optical Properties of materials," in *Optics*, YHLEE.
- [15] S. J. Orfanidis, "Oblique incidence in a lossy medium," in *Electromagnetic Waves and Antennas*, Sophocles J. Orfanidis, 2016.

- [16] F. D. Por, "Hydrobiological notes on the high-salinity waters of the Sinai Peninsula," *Springer: Marine Biology*, vol. 14, pp. 111-119, 1972.
- [17] S. Senda, "The Venice system for the classification of marine waters according to salinity : Symposium on the classification of brackish waters, Venice, 8-14 April 1958," Online Wiley Library, Venice.
- [18] E. Dahl, " Ecological salinity boundaries in poikilohaline waters," *oikos*, 1956.
- [19] Wikipedia, "Tyndall effect," Wikipedia the free encyclopedia, [Online]. Available: [https://en.wikipedia.org/wiki/Tyndall\\_effect](https://en.wikipedia.org/wiki/Tyndall_effect).
- [20] Encyclopedia Britannica, "Chemical and Physical Properties of Seawater," Encyclopedia Britannica.
- [21] C. E. W. R. M. Waxler, "Effect of Pressure and Temperature on the Refractive Indices of Benzene, Carbon Tetrachloride, and Water," *Journal of Research of the National Bureau of Standards Abbreviation Physics Chemistry*, vol. 67A, no. 2, pp. 163-171, 1963.
- [22] W. X. H. H. Z. CYang XE, " Mechanisms and assessment of water eutrophication.," *Journal of Zhejiang University-SCIENCE B- Springer*, vol. 9, no. 3, pp. 197-209, 2008 Mar.
- [23] R. C. Gonzalez, "Digital Image Processing, Vol3".
- [24] R. E. W. Rafeal C. Gonzalez, "Histogram Processing," in *Digital Image Processing*, Noida, UP, Pearson, 2013, pp. 120-121.
- [25] E. K. a. Z. A. A. M. F. Khan, "Segment dependent dynamic multi-histogram equalization for image contrast enhancement," *Digit. Signal Processing*, vol. 25, pp. 193-228, 2014.
- [26] T. C. a. T. Tjahjadi, "Contextual and variational contrast enhancement," *IEEE Trans. Image Process*, vol. 20, no. 12, pp. 3431-3441, 2011.
- [27] C. h. y. wei chih Yeh, "Image contrast enhancement for preserving mean brightness without losing image features," *Engineering Applications of Artificial Intelligence*, pp. 1487-1492, 2013.
- [28] G. Z. X. W. a. X. Y. H. Xu, "Generalized Equalization Model for Image Enhancement," *IEEE Transactions on Multimedia*, vol. 16, no. 1, pp. 68-82, 2014.
- [29] W. L. J. a. Z. Rong, "Image Defogging Algorithm of Single Color Image Based on Wavelet Transform and Histogram Equalization," *Applied Mathematical Sciences*, vol. 7, no. 79, pp. 3913 - 3921 , 2013.
- [30] M. F. Al-Sammarai, "Contrast enhancement of roads images with foggy scenes based on histogram equalization," in *10th International Conference on Computer Science & Education (ICCSE)*, 2015.



- [31] S. M. A. D. Badal Soni, "Foggy Image Enhancement Using Improved Histogram Equalization and Guided Filter," in *443-452*, 2022.
- [32] L.-P. & P. Z.-I. Yao, "The Retinex-based image dehazing using a particle swarm optimization method.," *Multimedia Tools and Applications*., 2021.
- [33] G. & P. K. Nam, "New Fuzzy-Based Retinex Method for the Illumination Normalization of Face Recognition.," *International Journal of Advanced Robotic Systems*. 9. 1-9. 10.5772/51664. , 2012.
- [34] J. Y. X. H. W. J. Q. Z. H. L. Qunfang Tang, "Nighttime image dehazing based on Retinex and dark channel prior using Taylor series expansion.," *Computer Vision and Image Understanding*., vol. 202, 2021.
- [35] J. T. Y. T. G. W. a. C. W. P. Li, ""Deep Retinex Network for Single Image Dehazing.," *IEEE Transactions on Image Processing*., vol. 30, pp. 1100-1115, 2021.
- [36] C. A. a. P. B. C. O. Ancuti, " "Effective single image dehazing by fusion.," in *IEEE International Conference on Image Processing*, 2010.
- [37] C. O. Ancuti and C. Ancuti, " "Single Image Dehazing by Multi-Scale Fusion.," *IEEE Transactions on Image Processing*, , vol. 22, no. 8, pp. 3271-3282, 2013.
- [38] L. M. J. Z. J. P. X. C. W. L. M.-H. Y. Wenqi Ren, "Gated Fusion Network for Single Image Dehazing," in *Proceedings of the IEEE Conference on Computer Vision and Pattern Recognition (CVPR)*., 2018.
- [39] R. D. Y. C. a. C. L. F. S. Fang, " "Effective single underwater image enhancement by fusion.," *J. Comput.*., vol. 8, no. 4, pp. 904-911, 2013.
- [40] X. L. Z. T. H. a. Y. F. J. H. Zhang, "Single image dehazing based on fast wavelet transform with weighted image fusion," in *IEEE Int. Conf. Image Processing*, Paris, France, 2014.
- [41] J.-P. T. D. A. a. E. D. N. Hautiere, "Blind Contrast enhancement assessment by gradient ratioing at visible edges," *IEEE TRANSACTIONS ON IMAGE PROCESSING*., vol. 22, no. 8, pp. 1057-7149, AUGUST 2013.
- [42] [Online]. Available: <http://www.owl.net.rice.edu/~elec539/Projects99/BACH/proj2/intro.html>.
- [43] W. W. a. X. Yuan, "Recent Advances in Image Dehazing.," *IEEE/CAA J. Autom. Sinica*., vol. 4, no. 3, pp. 410-436, 2017.
- [44] J. Y. ., J. W. Ketan Tang, "Investigating Haze-relevant Features in A Learning Framework," in *IEEE Conference on Computer Vision and Pattern Recognition*, 2014.
- [45] J. S. a. X. T. Kaiming He, "Single image haze removal using dark channel prior," in *IEEE Conference on Computer Vision and Pattern Recognition*., 2009 .

- [46] S. J. B. a. T. Q. N. Kristofor B. Gibson, "Example based depth from fog," in *20th IEEE International Conference on Image Processing (ICIP)*, 2013.
- [47] J. M. M. a. L. S. Q. S. Zhu, ", "Single image dehazing using color attenuation prior, ", " in *25th British Machine Vision Conference*,, 2014.
- [48] J. M. M. a. L. S. Q. S. Zhu, ""A fast single image haze removal algorithm using color attenuation prior,," " *IEEE Trans. Image Process.*,, vol. 24, no. 11, pp. 3522-3533, 2015.
- [49] R. T. Tan, ", "Visibility in bad weather from a single image,," in " in *Proc. 2008 IEEE Conf. Computer Vision and Pattern Recognition*, , Anchorage, AK, USA, , 2008.
- [50] C. A. a. C. O. Ancuti, ", "Effective contrast-based dehazing for robust image matching, ", " *IEEE Geosci. Remote Sens. Lett.*, , vol. 11., no. 11, pp. 1871-1875, 2014.
- [51] J. P. H. K. a. J. P. Hasil Park, "Variational Image Dehazing using a Fuzzy Membership Function," *IEIE Transactions on Smart Processing and Computing*, , vol. 6, no. 2, 2017.
- [52] C. W. Z. X. a. R. W. L. Q. Shu, ""Variational regularized transmission refinement for image dehazing,," in *IEEE International Conference on Image Processing (ICIP)*, Taipei, Taiwan, 2019.
- [53] M. J. M. Kang, "A single image dehazing model using total variation and inter-channel correlation.,," *Multidimensional System Signal Processing, Springer*, vol. 31, pp. 431-464, 2020.
- [54] V. D. K. V. P. Monika Verma, "Fog Removal by Multiple Polynomial Regression Model through Curvelets," *International Journal of Intelligent Engineering and Systems* , vol. 10, no. 5, pp. 201-209, October 2017.
- [55] H. K. e. all., ""Localization of radiance transformation for image dehazing in wavelet domain,," *Neurocomputing, Elsevier*, vol. 381, p. 141–151, 2020.
- [56] H. L. Y. Y. J. C. a. K. W. M. Fu, ""DW-GAN: A discrete wavelet transform GAN for nonhomogeneous dehazing,," in *IEEE Conference on Computer Vision and Pattern Recognition (CVPR)* , 2021.
- [57] W. -Y. Hsu and Y. -S. Chen, ""Single Image Dehazing Using Wavelet-Based Haze-Lines and Denoising,," *IEEE Access*, vol. 9, pp. 104547-104559,.
- [58] M. B. a. H. R. C. Hodges, ""Single image dehazing using deep neural networks,,"" *Pattern Recognition Letters*, vol. 128, pp. 70-77, 2019.
- [59] H. Z. Y. -M. C. X. Y. a. Y. Y. T. X. Liu, ""Efficient single image dehazing and denoising: An efficient multi-scale correlated wavelet approach,,"" *Computer Vision and Image understanding*, vol. 162, pp. 23-33, 2017.

- [60] F. Z. X. R. Y. a. C. Z. J. He, "Fast single image dehazing via multilevel wavelet transform based optimization," *Cornel University, ARXIV*, 2019.
- [61] X. X. K. J. C. Q. a. D. T. B. Cai, "DehazeNet: An end-to-end system for single image haze removal," *IEEE Transactions on Image Processing*, vol. 25, no. 11, pp. 5187-5196, 2016.
- [62] G. L. a. H. F. J. Li, "Image dehazing using residual-based deep CNN," *IEEE Access*, vol. 6, pp. 26831-26841, 2018.
- [63] J. L. a. N. X. K. Yuan, "Single image dehazing via NIN dehazenet," *IEEE Access*, vol. 7, pp. 181348-181356, 2019.
- [64] J. H. P. X. Z. C. a. M.-H. Y. W. Ren, "Single image dehazing via multi-scale convolutional neural networks with holistic edges," *International Journal of Computer Vision, (IJCV), Springer*, vol. 128, no. 1, pp. 240-259, 2020.
- [65] Z. H. C.-C. T. a. C.-W. L. Q. Deng, "HardGAN: A haze-aware representation distillation GAN for single image dehazing," in *European Conference on Computer Vision (ECCV)*, 2020.
- [66] M. S. J. L. J. Z. R. K. a. H. G. S. J. Xiao, "Single image dehazing based on learning of haze layers," *Neurocomputing, Elsevier*, vol. 389, pp. 108-122, 2020.
- [67] A. G. a. H. K. E. D. Engin, "Cycle-dehaze: Enhanced cycleGAN for single image dehazing," in *IEEE Conference on Computer Vision and Pattern Recognition*, 2018.
- [68] Z. G. C. C. H. A. H. L. T. a. K. C. Y. Z. Su, "Prior guided conditional generative adversarial network for single image dehazing," *Neurocomputing, Elsevier*, vol. 423, pp. 620-638, 2021.
- [69] L. L. e. al., "Semi-supervised image dehazing," *IEEE Transactions on Image Processing*, vol. 29, pp. 2766-2779, 2020.
- [70] W. F. Y. W. a. Z. S. C. Wang, "Weakly supervised single image dehazing," *Journal of Visual. Communication and Image Representation*, vol. 72, 2020.
- [71] A. S. a. R. T. T. W. Yan, "Optical flow in dense foggy scenes using semi-supervised learning," in *IEEE/CVF Conferences on Computer Vision and Pattern Recognition*, 2020.
- [72] X. L. H. L. a. Z. Z. S. An, "Semi-supervised image dehazing network," *The Visual Computer, Springer*, vol. 12, pp. 1-15, 2021.
- [73] Y. C. J. H. a. Y. X. Y. Qu, "Enhanced Pix2pix dehazing network," in *Proceedings of IEEE/CVF Conference of Computer Vision & Pattern Recognition*, 2019.

- [74] J. S. a. X. T. K. He, "Single hazy image haze removal using dark channel prior," *IEEE Transactions on Pattern Analysis and Machine Intelligence*, vol. 33, no. 12, pp. 2341-2353, 2011.
- [75] J. M. R. A. J. C. P. -O. a. J. R.-R. S. Salazar Colores, "Efficient Single Image dehazing by modifying dark channel prior," *EURASIP Journal of Image Video Processing*, vol. 2019, pp. 1-8, 2019.
- [76] M. L. X. W. a. D. Z. C. Dai, "Single Hazy Image Restoration using robust atmospheric scattering model," *Signal Processing*, vol. 166, no. Art. No.:107257, 2020.
- [77] V. K. V. C. B. K. S. S. T. Hassène Gritli, "Efficient Single Image Dehazing Model Using Metaheuristics-Based Brightness Channel Prior," *Mathematical Problems in Engineering, Hindawi*, 2021.
- [78] V. J. D. Almero et al., ""Genetic Algorithm-based Dark Channel Prior Parameters Selection for Single Underwater Image Dehazing,"" in *IEEE REGION 10 CONFERENCE, (TENCON)*, 2020.
- [79] H. T. Z. L. Q. W. W. L. X. N. Z. J. M. Z. Wu, "An Image Dehazing Algorithm Based on Single-Scale Retinex and Homomorphic Filtering," *Communications, Signal Processing, and Systems. CSPA 2019. Lecture Notes in Electrical Engineering*, vol. 571, no. Singapore, 2019.
- [80] H. L. X. L. Q. e. a. Yu, "Underwater image enhancement based on DCP and depth transmission map.," *Multimed Tools Applications*, vol. 79, p. 20373–20390, 2020.
- [81] H. L. X. L. Q. e. a. Yu, "Underwater image enhancement based on color-line model and homomorphic filtering.,," *Signal, Image and Video Processing*, pp. 83-91, 2022.
- [82] H. Yang and Y. Fu, ""Wavelet U-Net and the Chromatic Adaptation Transform for Single Image Dehazing,"" in *IEEE International Conference on Image Processing (ICIP), 2019, pp. 2736-2740.*, 2019.
- [83] G. Z. Jinhua Li, "Wind turbine blade surface crack image enhancement based on Curvelet Transform," *International Core Journal of Engineering*, vol. 5, no. 5, pp. 2414-1895, 2019.
- [84] W. K. M. T. M. U. M. C. Neel Joshi, "Real-Time Hyperlapse Creation Via Optimal Frame Selection`," *ACM Transactions on Graphics (TOG) - Proceedings of ACM SIGGRAPH 2015*, vol. 34, July 2015.
- [85] M. C. a. R. S. Johannes Kopf, "First Person Hyper-Lapse Videos," *ACM Transactions on Graphics (Proc. SIGGRAPH 2014)*, 2014 August.
- [86] B. Z. e. a. Ziyu Wan, "Enhancing your photos through Artificial Intelligence," *Computer Vision and Pattern Recognition (CVPR2020)*, 2020.

- [87] C. S. e. all., "Photorealistic Text-to-Image Diffusion Models with Deep Language Understanding," *Computer Vision and Pattern Recognition (CVPR)*, 2022.
- [88] e. a. Haitian Zheng, "CM-GAN: Image Inpainting with Cascaded Modulation GAN and Object-Aware Training," *ECCV2022*, 2022.
- [89] e. a. Anna Frühstück, "InsetGAN for Full-Body Image Generation," *CVPR2022*, 2022.
- [90] Computer Vision Group (CVG), University of Granada (CVG-URG), "TEST IMAGES," University of Granada, 13 03 2014. [Online]. Available: <https://ccia.ugr.es/cvg/dbimagenes/>. [Accessed 04 09 22].
- [91] University of Southern California (USC), "USCViterbi School of Engineering.," Signal and Image Processing Institute (SIPI). Ming Hsieh Department of Electrical and Computer Engineering., [Online]. Available: <https://sipi.usc.edu/database/>. [Accessed 04 09 2022].
- [92] Eastman Kodak Company, "Kodak Lossless True Color Image Suite," Eastman Kodak Company, 1999 to 2013. [Online]. Available: <http://r0k.us/graphics/kodak/>. [Accessed 04 09 2022].
- [93] C. F. a. D. M. Pablo Arbelaez, "The Berkeley Segmentation Dataset and Benchmark," University of California, Berkeley, June 2007. [Online]. Available: <https://www2.eecs.berkeley.edu/Research/Projects/CS/vision/bsds/>. [Accessed 04 09 2022].
- [94] University of South Florida, "DDSM: Digital Database for Screening Mammography," University of South Florida, 2006. [Online]. Available: <http://www.eng.usf.edu/cvprg/Mammography/Database.html>. [Accessed 04 09 2022].
- [95] A. M. Martinez, "AR Face Database," Ohio State University, 06 1998. [Online]. Available: [https://www2.ece.ohio-state.edu/~aleix/ARdatabase.html#:~:text=This%20face%20database%20was%20created,70%20men%20and%2056%20women\)..](https://www2.ece.ohio-state.edu/~aleix/ARdatabase.html#:~:text=This%20face%20database%20was%20created,70%20men%20and%2056%20women)..) [Accessed 04 09 2022].
- [96] W. R. Z. W. Boyi Li, "RESIDE A Benchmark for Single Image Dehazing," *IEEE Transactions on Image Processing*, vol. 14, no. 8, 2019.
- [97] B. a. R. W. a. F. D. a. T. D. a. F. D. a. Z. W. a. W. Z. Li, "Benchmarking Single-Image Dehazing and Beyond," *IEEE Transactions on Image Processing*, vol. 28, no. 1, pp. 492-505, 2019.
- [98] N. H. A. C. D. G. a. H. H. J.-P. Tarel, "Improved Visibility of Road Scene Images under Heterogeneous Fog," *Proceedings of IEEE Intelligent Vehicles Symposium (IV'10)*, vol. 2, pp. 6-20, 2012.
- [99] Kaggle, "Kaggle-Flickr Image Captioning Dataset," Kaggle, [Online]. Available: <https://www.kaggle.com/datasets/hsankesara/flickr-image-dataset>. [Accessed 04 09 2022].

- [100] N. a. CVPR, "7th New Trends in Image Restoration and Enhancement workshop and challenges 2022," NTIRE and CVPR, 2022.
- [101] NTIRE, "NTIRE2016," NTIRE, Taipei, Taiwan, 20 November, 2016.
- [102] NTIRE, "NTIRE2017," NTIRE, Honolulu, Hawaii, 2017.
- [103] NTIRE, "NTIRE2018," NTIRE and CVPR, Salt Lake City, Utah, 2018.
- [104] NTIRE, "NTIRE2019," CVPR and NITRE, Long Beach, California, 2019.
- [105] NITRE, "NITRE2020," CVPR and NITRE, Seattle, Washington, 2020.
- [106] NITRE, "NITRE2021," NITRE, CVPR, Virtual, US, 2021.
- [107] A. G. a. P. L. a. C. S. a. R. Urtasun, "Vision meets Robotics: The KITTI Dataset," *International Journal of Robotics Research (IJRR)*, 2013.
- [108] R. F. D. H. P. K. Nathan Silberman, "Indoor Segmentation and Support Inference from RGBD Images," *Computer Vision-ECCV12, Springer*, 2012.
- [109] "Middlebury Stereo Dataset," 2001-2021. [Online]. Available: <https://vision.middlebury.edu/stereo/data/>.
- [110] F. S. R. S. Z. R. C. C. T. Ergys Ristani, "Performance Measures and a Data Set for Multi-Target, Multi-Camera Tracking," *ECCV 2016 Workshop on Benchmarking Multi-Target Tracking*, 2016.
- [111] J. Y. a. A. C. B. L. K. Choi, "Referenceless Prediction of Perceptual Fog Density and Perceptual Image Defogging," *IEEE Transactions on Image Processing*, vol. 24, no. 11, pp. 3888-3901, 2015.
- [112] W. & Y. X. Wang, "Recent advances in image dehazing.," *IEEE/CAA Journal of Automatica Sinica*, pp. 410-436., 2014.
- [113] Wikipedia Contributors, "Pyramid (Image Processing)," Wikipedia, The Free Encyclopedia, 26 June 2022. [Online]. Available: [https://en.wikipedia.org/w/index.php?title=Pyramid\\_\(image\\_processing\)&oldid=1095183621](https://en.wikipedia.org/w/index.php?title=Pyramid_(image_processing)&oldid=1095183621). [Accessed 28 October 2022].
- [114] Z.-u. R. G. A. W. Daniel J. Jobson, "A Multiscale Retinex for Bridging the Gap Between Color Images and the Human Observation of Scenes," *IEEE TRANSACTIONS ON IMAGE PROCESSING*, vol. 6, no. 7, pp. 965-976, 1997.
- [115] S. S. V. Dalvi, "Improved weight map guided single image dehazing," in *IJERT-IEEE*, 2016.
- [116] C. O. A. a. C. A. a. M. S. a. R. Timofte, "Dense-Haze\_2019, Dense haze: A benchmark for image dehazing with dense-haze and haze-free images," in *IEEE International Conference on Image Processing (ICIP)*, Taipei, Taiwan, 2019.

- [117] A. B. Petro, C. Sbert and J.-M. Morel, "Multiscale Retinex," *Image Processing On Line*, pp. 71-88, 2014.

## LIST OF PUBLICATIONS

1. P. Purkayastha, M. S. Choudhary and M. Kumar, "Steerable Pyramid-based Multi-Scale Fusion Algorithm for Single Image Dehazing," *2023 International Conference on Device Intelligence, Computing and Communication Technologies, (DICCT)*, Dehradun, India, 2023, pp. 552-557, doi: 10.1109/DICCT56244.2023.10110293. [Published]
2. P. Purkayastha, M. S. Choudhary and M. Kumar, "Steerable Pyramid-based Multi-Scale Fusion Algorithm for Single Image Dehazing," *2023 International Conference on Recent Advances in Electrical, Electronics and Digital Healthcare Technologies (REEDCON)*, Delhi, India, 2023 [Submitted, Accepted]





Graphic Era  
Deemed to be  
University  
DEHRADUN



Department of  
Electronics & Communication  
Engineering

International Conference on  
Device Intelligence, Computing, and Communication Technologies  
(DICCT-2023) March 17-18, 2023

## Certificate of Participation

This is to certify that

Mr./Ms./Dr./Prof. PAULANI PURKAYASTHA

from DELHI TECHNOLOGICAL UNIVERSITY, NEW DELHI, Dept ECE

has participated and presented the paper titled - STEERABLE PYRAMID - BASED

MULTI-SCALE FUSION ALGORITHM FOR SINGLE IMAGE DEHAZING

in the International Conference on **Device Intelligence, Computing, and  
Communication Technologies (DICCT-2023)** on **March 17-18, 2023**

organised by the Department of Electronics & Communication Engineering,  
Graphic Era Deemed to be University, Dehradun, Uttarakhand, India

Dr. Mridul Gupta  
Convener

Prof. (Dr.) Shalini Singh  
Technical Program Chair

Prof. (Dr.) Md. Irfanul Hasan  
Conference Chair



**REEDCON  
2023**



C. No. REEDCON 2023/EED/JMI/3004

**International Conference  
on**

***Recent Advances in Electrical, Electronics & Digital Healthcare Technologies  
REEDCON 2023***

Organized by

**Department of Electrical Engineering, Jamia Millia Islamia, New Delhi**

***Certificate of Presentation***

Prof./Dr./Ms./Mr. **Paulami Purkayastha** of **Delhi Technological University** has presented a paper titled as **A Retinex Prior to Multi-Scale Fusion for Single Image Dehazing** at the **International Conference on Recent Advances in Electrical, Electronics & Digital Healthcare Technologies, 2023 (REEDCON 2023)** during **01<sup>st</sup> – 03<sup>rd</sup> May, 2023** at Jamia Millia Islamia, New Delhi.

**(Prof. Munna Khan)**  
Organizing Chair

**(Prof. Majid Jamil)**  
Organizing Secretary

## M-Tech thesis

### ORIGINALITY REPORT

|                  |                  |              |                |
|------------------|------------------|--------------|----------------|
| <b>13%</b>       | <b>9%</b>        | <b>9%</b>    | <b>0%</b>      |
| SIMILARITY INDEX | INTERNET SOURCES | PUBLICATIONS | STUDENT PAPERS |

### PRIMARY SOURCES

|           |  |               |
|-----------|--|---------------|
| <b>1</b>  | <b>dspace.dtu.ac.in:8080</b><br>Internet Source  | <b>2%</b>     |
| <b>2</b>  | <b>Geet Sahu, Ayan Seal, Debotosh Bhattacharjee, Mita Nasipuri, Peter Brida, Ondrej Krejcar. "Trends and Prospects of Techniques for Haze Removal From Degraded Images: A Survey", IEEE Transactions on Emerging Topics in Computational Intelligence, 2022</b><br>Publication | <b>1%</b>     |
| <b>3</b>  | <b>dokumen.pub</b><br>Internet Source  | <b>1%</b>     |
| <b>4</b>  | <b>www.researchgate.net</b><br>Internet Source   | <b>1%</b>     |
| <b>5</b>  | <b>www.hindawi.com</b><br>Internet Source  | <b>&lt;1%</b> |
| <b>6</b>  | <b>digital-photography-school.com</b><br>Internet Source   | <b>&lt;1%</b> |
| <b>7</b>  | <b>www.mdpi.com</b><br>Internet Source   | <b>&lt;1%</b> |
| <b>8</b>  | <b>"Table of Contents", 2023 International Conference on Device Intelligence, Computing and Communication Technologies, (DICCT), 2023</b><br>Publication   | <b>&lt;1%</b> |
| <b>9</b>  | <b>Abdul Jabbar, Xi Li, Muhammad Assam, Javed Ali Khan et al. "AFD-StackGAN: Automatic Mask Generation Network for Face De-Occlusion Using StackGAN", Sensors, 2022</b><br>Publication   | <b>&lt;1%</b> |
| <b>10</b> | <b>www.coursehero.com</b><br>Internet Source   | <b>&lt;1%</b> |
| <b>11</b> | <b>link.springer.com</b><br>Internet Source  | <b>&lt;1%</b> |
| <b>12</b> | <b>Yaozong Mo, Chaofeng Li, Yuhui Zheng, Xiaojun Wu. "DCA-CycleGAN: Unsupervised</b>   | <b>&lt;1%</b> |